ACS Photonics

Perspective

pubs.acs.org/journal/apchd5

Plasmonic Nanoparticle Enhancement of Solution-Processed Solar Cells: Practical Limits and Opportunities

Ebuka S. Arinze,[†] Botong Qiu,[†] Gabrielle Nyirjesy,[‡] and Susanna M. Thon*[,†]

[†]Department of Electrical and Computer Engineering and [‡]Department of Materials Science and Engineering, Johns Hopkins University, Baltimore, Maryland 21218, United States

ABSTRACT: Solution-processed solar cells are particularly suited to benefit from absorption enhancement by plasmonic nanoparticles, due to their transport-limited film thicknesses and the ease with which metal nanoparticles can be integrated into the materials. Despite practical demonstrations of performance enhancements, the overall benefits have so far been limited in scope to photocurrents well below the theoretical limits. In this Perspective, we critically evaluate the prospects for plasmonic enhancements in solution-processed thin-film solar cells. We give an overview of recent work, focusing on embedded plasmonic nanoparticles in organic, perovskite, and colloidal quantum dot solar cells. We then develop an intuitive effective medium model for embedded plasmonic nanostructures in photovoltaic thin films, evaluate the model in the context of previous results in the field, and use the model to provide a framework for identifying the most promising avenues for realizing plasmonic performance enhancements in solution-processed solar cells. Our results indicate that further plasmonic enhancement gains may be possible in organic photovoltaic cells, whereas concentrating on improving transport in perovskite and colloidal quantum dot architectures is a more promising route to performance advances. Additionally, fine-tuning the concentration of plasmonic enhancers within the absorbing medium is critical for achieving maximum photocurrent potential.

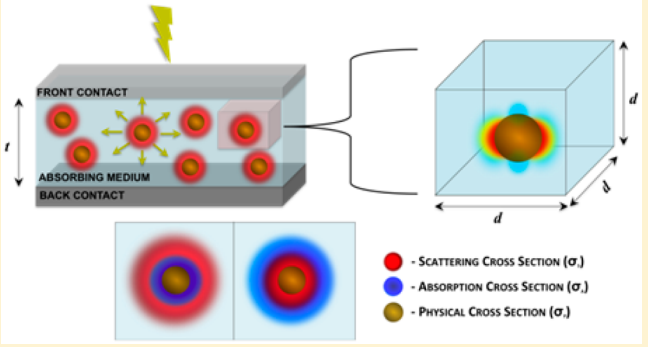

KEYWORDS: *plasmonics, photovoltaics, light trapping, solution processing, organic photovoltaics, perovskites, colloidal quantum dots*

The search for sustainable and cost-competitive alternatives to fossil fuel-based energy sources has driven developments in solution-processed solar cells. These technologies seek to reduce manufacturing and processing costs as well as improve device efficiencies over traditional and thin-film bulk semiconductor platforms. The low-temperature roll-to-roll production methods, solution-based fabrication techniques, and high-efficiency potential make materials such as polymers,[1−5] hybrid perovskites,[6−10] and colloidal quantum dots[11−16] attractive technologies. However, the electronic transport lengths in most solution-processed materials are smaller than the photon absorption lengths, especially at near-infrared wavelengths, due to their nanostructured nature and associated interface-related defects and impurities. This is referred to as the "absorption−extraction compromise", whereby the material thickness required for complete absorption results in incomplete extraction of the photogenerated charge carriers.

Attempts to improve the efficiencies of solution-processed devices have included engineering of the absorbing material,[17−20] design of new device architectures,[21−25] and incorporation of light-trapping techniques to decrease the effective film absorption lengths.[26−31] Introducing plasmonic elements, which enhance the interaction of light with matter in metallic structures on the nanoscale, has been of particular interest to the field due to their minimum perturbation of the device structure and successful deployment for related optoelectronic device applications.[32−37]

Various efforts to introduce plasmonic enhancers into solution-processed photovoltaic cells have been tested, some of which will be reviewed in the following section. However, absolute photocurrent and power conversion efficiency improvements have been relatively limited thus far, partially due to the difficulty in systematic evaluation of the optimum plasmonic nanoparticle design for integration with specific photovoltaic materials. Here, we provide an overview of the field of embedded plasmonic-enhanced solution-processed solar cells. We then develop an analytical model to systematically evaluate the practical potential of plasmonic enhancements in thin-film materials. We compare the photocurrent enhancements predicted by our model to simulation and experimental results for three different systems. Finally, we use our model to make specific suggestions for the field moving forward, focusing on the optimum plasmonic nanoparticle material type, material shape, and concentration for realizing maximum potential enhancements for different systems.

Received: September 1, 2015
Revised: December 29, 2015
Accepted: December 29, 2015
Published: December 29, 2015

DOI: 10.1021/acsphotonics.5b00428
ACS Photonics 2016, 3, 158−173

SOLUTION-PROCESSED SOLAR CELLS

Compared to traditional bulk semiconductors, solution-processed solar cell materials typically have shorter charge transport lengths, stronger exciton binding energies, and larger electronic trap state densities due to the heterogeneity of their structures arising from the low-energy fabrication and processing procedures. Additionally, flexibility in doping of the materials is generally lacking. Therefore, solution-processed solar cell architectures have been designed to engineer around these issues. Taking inspiration from electrochemical cells, most solution-processed photovoltaic devices employ heterointerfaces, which can be structured to enhance charge separation and collection while minimizing the thickness of the active material.

Initial organic photovoltaic (OPV) architectures involving a bilayer donor−acceptor planar heterojunction[38] suffered from the "exciton-diffusion" bottleneck that resulted from the small diffusion lengths.[39−43] This led to the development of the bulk heterojunction architecture, in which the acceptor and donor phases are blended to form a high interfacial area mixture.[44,45] This architecture is limited by the ability to optimally distribute charge separation interfaces and facilitate appropriate conduction channels.[46−48]

The highest-performing colloidal quantum dot (CQD) photovoltaic devices use a heterojunction architecture in which the CQD medium forms a junction with an n-type wide band gap semiconductor such as TiO_2 or ZnO.[49] Control over the CQD film doping,[50] band alignment,[51] and structuring of the electrodes[52] has led to the development of advanced architectures that utilize multiple CQD film types, although high electronic trap state densities still limit performance.[53]

In the case of perovskite solar cells, sensitizing-type architectures produced most of the initial results in the field. The perovskite material is infiltrated into an electron-extracting[25,54−57] or insulating[58−60] mesoporous layer (usually TiO_2 and Al_2O_3, respectively) and topped with a hole-transporting material. With advances in the growth of long-diffusion-length large-domain single-crystal perovskites,[61,62] the field is trending toward more conventional planar cell designs in which the perovskite film is sandwiched between electron- and hole-extracting electrodes.

The limited carrier transport lengths necessitate careful engineering of solution-processed solar cell device architectures in order to maximize absorption and achieve the highest possible efficiencies. This problem is magnified at longer photon wavelengths near the band gap energy where absorption lengths can exceed carrier transport lengths by more than an order of magnitude in OPV and CQD materials, making light trapping a vital component of successful device designs.

LIGHT TRAPPING FOR PHOTOVOLTAICS

As a technique for absorption enhancement, the idea of light trapping in thick and thin optical films has been studied for decades.[63−66] Conventionally, light trapping employs total internal reflection as the primary confinement mechanism and is achieved through structural manipulation of the device layers. The maximum absorption enhancement factor (Yablonovitch limit or Lambertian limit[63−65]) for conventional thin-film light-trapping strategies is $4n^2/\sin^2\theta$, where n is the refractive index of the absorbing medium and θ is the angle of the emission cone in the medium surrounding the cell (also known as the acceptance angle). For normal incidence radiation ($\theta = \pi/2$), this upper limit can be further simplified to $4n^2$.

Recent theoretical work on light trapping has focused on the ultra-subwavelength regime for optical film thicknesses. On the nanoscale, where light−matter interactions beyond the classical ray optics limit take place, it is theoretically possible to surpass the traditional Lambertian limit over specific wavelength ranges.[57] Using a rigorous electromagnetic approach, Yu et al. developed a statistical temporal coupled-mode theory of light trapping,[67] demonstrating that the enhancement factor can in theory be increased to $12 \times 4n^2$ over a virtually unlimited spectral bandwidth when optical modes exhibit deep-subwavelength-scale field confinement. Callahan et al. proposed that an elevated local density of optical states (LDOS) for the absorber is the key design element, and they demonstrated several nanostructured solar cell architectures that exceeded the Yablonovitch limit in simulation.[68]

Beyond evaluating the absorption enhancement factor, Schuster et al. proposed a figure of merit called light-trapping efficiency (LTE), which is the ratio of the total current gain achieved in a device to the theoretical maximum current gain achievable in an ideal Lambertian scattering system.[69] Using LTE as a metric, they demonstrated that multiple theoretical and experimental photonic structures could be used to approach the enhancement limit.[69] Plasmonic enhancement strategies ideally fall under the category of approaches that can be used to exceed the Lambertian limit.

EMBEDDED PLASMONIC ENHANCERS

The collective oscillations of the free electrons at the surface of a conductor are known as surface plasmons. These excitations couple strongly to incident electromagnetic radiation and are able to propagate along a metal−dielectric interface as surface plasmon polaritons. Plasmons can be excited at optical frequencies in materials such as gold and silver. In nanoscale structures, localized surface plasmon resonances (LSPRs) result in strong local field enhancement. This nanophotonic effect can be used to circumvent the traditional diffraction limits and can result in the scattering of incoming light into guided modes in a thin-film material with embedded plasmonic nanoparticles. Plasmonic elements have been applied in diverse applications such as nanoscale sensing,[70−72] light-emitting diodes,[73−75] lasers,[76−78] photon detection,[79] information processing,[80] and photovoltaics.[30,81−85]

Embedded plasmonic structures are of particular interest for solution-processed photovoltaic devices, such as those based on organic, hybrid inorganic−organic perovskite, and colloidal quantum dot thin-film materials. Several reports study the integration of plasmonic structures into such devices with demonstrated increases in optical absorption.[81,82,84,86] Embedded plasmonic structures within the absorbing medium are of particular interest for solution-processed technologies since the materials growth techniques are uniquely compatible with hybrid inclusions, whereas bulk semiconductor systems must rely on surface-based plasmonic in-couplers or scatterers.[87−92]

Plasmonic nanostructures can be spatially placed at the top of, within, or at the base of solution-processed devices. Placing the plasmonic nanoparticles within the active layer rather than in or on top of contact or buffer layers has several advantages. Mixing the plasmonic materials into the active layer of the cell can help to reduce reflection losses that occur before the light reaches the active layer and increase wave-guiding within the absorbing medium.[93−95] Finally, the near-field effects associated with LSPRs can be used to enhance absorption within the active layer if there is a strong spatial-field overlap with the

DOI: 10.1021/acsphotonics.5b00428
ACS Photonics 2016, 3, 158−173

Table 1. Summary of Selected Plasmonic Enhancement Demonstrations in OPV (Red), Perovskite (Green), and CQD (Purple) Solar Cells

Plasmonic Material (Shape)	*Plasmonic Nanoparticle Size (nm)*	*Plasmonic Nanoparticle Concentration*	*Max. J_{SC} (mA/cm^2)*	*J_{SC} Enhancement*	*Max. PCE (%)*	*PCE Enhancement*
Au (Octahedron)[121]	45	2×10^{11} cm^{-3}	10.22	11.6%	4.24	18.8%
Au (Sphere)[111]	30-40	20% by vol.	10.18	13.7%	4.19	20.4%
Au (Truncated Octahedron)[93]	70	5 wt.%	11.16	8.3%	6.45	11.8%
Ag (Nanocluster)[94]	40	1 wt.%	11.61	7.6%	7.1	12.7%
Au (Sphere)[95]	18	0.5 wt.%	4.8	15.7%	2.17	32.3%
Ag (Sphere)[122]	5 to 15	1:16 wt. ratio (Ag: P3HT)	8.9	1.1%	3.3	-2.9%
Au (Truncated Octahedron) [123]	80	15 wt.%	8.7	19.2%	3.2	88.2%
Ag (Sphere and Prism)[124]	20 and 60 x 10	2 wt.%	10.61	18%	4.3	19.4%
Au (Sphere)[125]	30	1 wt.%	15.3	-0.1%	7.02	6.7%
Au-Ag (Popcorn Alloy)[126]	150±50	0.7 wt.% TiO_2	16.46	6.1%	10.3	15.7%
Au-SiO2 (Sphere)[31]	80/8 (core/ shell)	.9 wt.%	15.3	13.5%	9.5	13%
Ag-TiO2 (Sphere)[108]	40/2 (core/ shell)	2.2 wt.%	22	8.9%	16.3	12.4%
Au (Sphere)[134]	5	.3% by vol.	29.45	42.2%	4.5	12.5%
Ag (Hemisphere)[135]	40	33% surface coverage	8.5	19.4%	0.68	58.1%
SiO2-Au (Core-Shell Sphere)[107]	15/60 (core/ shell)	10 μm^{-2}	24.5	13%	6.9	11%

absorbing medium. Embedded plasmonic schemes make use of this strong local field enhancement without significantly disrupting the device structure as in conventional light-trapping designs.

While this perspective focuses on embedded nanoparticle plasmonic enhancement strategies, nonembedded plasmonic strategies have been explored in-depth in the field, due to the ease of design and fabrication associated with integrating top- and bottom-device structures without disrupting the active layers. These schemes include placing metallic nanoparticles and nanostructured gratings outside the active layers for light in-coupling and trapping.[96−105] Symmetric metallic nanostructured gratings, either 1D or 2D nanostructures, can be designed for effective light coupling to surface plasmon polariton (SPP) modes that strongly confine light at the interface, resulting in light concentration or preferential scattering into the active layer.

Examples of these methods include the design and integration of 2D SPP gratings for incident light coupling at the exciton peak wavelength in a CQD optoelectronic device.[105] A peak absorption enhancement factor of 3 was observed at the target wavelength. Additionally, the short-circuit current in the light-trapping spectral range (640 to 1100 nm) was observed to increase by 41%. In another study for OPVs,[102] a 14.8% improvement in efficiency was observed due to the integration of Ag nanoparticle films at the front electrode for preferential forward scattering into the active layer. In this plasmonic scheme, the Ag nanoparticle film was self-assembled via thermal evaporation and subsequent annealing.

In general, the propensity of plasmonic nanoparticles embedded within the active layer itself to serve as recombination sites for exciton quenching[106] has led to extensive exploration of plasmonic enhancement schemes that take advantage of scattering and light coupling from the electrode layers. However, the potential for high near-field enhancements from plasmonic particles embedded within the active layer provides motivation for further exploring embedded nanoparticle schemes.

The field of embedded plasmonic enhancement schemes for solution-processed solar cells has advanced rapidly in recent years. Plasmonic particles of different shapes and sizes have been studied in organic photovoltaic, colloidal quantum dot, and perovskite solar cells. Large photocurrents have been demonstrated, although relative power conversion efficiency (PCE) enhancements have remained less than 16% for films with PCE values of more than 5%.

Table 1 summarizes the progress so far in embedded plasmonic enhancement schemes for solution-processed solar cells. Gold and silver are the most commonly used plasmonic materials, and they have also been combined with oxide cores or shells.[31,107,108] The nanoparticles in the summarized studies ranged in size from 5 to 150 nm and were embedded at concentrations of 1−15 wt %. The maximum PCE of 16.3% was achieved in a perovskite solar cell.[108] Maximum PCEs of 7.1% and 6.9% were achieved through plasmonic enhancement in OPVs and CQD solar cells, respectively.[94,107] Although many potential nanoplasmonic enhancement schemes have been explored,[32,84,85,87,108−115] experimental realizations of integrated plasmonic designs have yet to lead to record device efficiencies.[116−120]

Organic Photovoltaics. Plasmonic particles have been embedded within or between the active layers and selective contacts in OPV devices.[93−95,111,121−125] Typical OPVs have an active layer that consists of electron-donor and electron-acceptor materials.

One study[94] incorporated chemically synthesized 40 nm silver nanoclusters into the active layer of a poly[*N*-9″-heptadecanyl-2,7-carbazole-*alt*-5,5-(4′,7′-di-2-thienyl-2′,1′,3′-benzothiadiazole) (PCDTBT):[6,6]-phenyl-C_{70}-butyric acid methyl ester ($PC_{70}BM$) bulk heterojunction (BHJ) solar cell to improve the efficiency. The nanoclusters exhibited a

DOI: 10.1021/acsphotonics.5b00428
ACS Photonics 2016, 3, 158−173

maximum absorbance peak near 420 nm. A 12.7% improvement in PCE was obtained by optimizing the weight percentage of the nanoclusters in the active layer. This enhancement was mainly due to a 7.6% increase in the short-circuit current density (J_{SC}) and an associated reduction in the cell series resistance.

The addition of 70 nm truncated gold octahedral nanoparticles at optimized concentrations (5 wt %) to the BHJ active layer in another study[93] resulted in consistent PCE improvements in fabricated devices. Other shapes, including Ag nanoparticles and nanoprisms mixed into the buffer layer of an OPV cell,[124] have also been used to realize wide-band absorption enhancements. Generally, relative PCE improvements on the order of 10% have been demonstrated in plasmonically enhanced OPV devices, mainly due to increases in J_{SC}. Associated compromises in the open-circuit voltage (V_{OC}) and fill factor (FF) are the prime reasons that these systems have been unable to rival the record efficiencies in the field.

Perovskite Solar Cells. Embedded plasmonic schemes have been explored only recently in perovskite solar cells, due to the relative novelty of this technology.[31,108,126] One demonstration enhanced the PCE of a perovskite solar cell by 12.4% by incorporating 40 nm silver-core nanoparticles with 2 nm TiO_2 shells through a low-temperature processing route.[108] The nanoparticles were added to the mesoporous Al_2O_3 scaffold layer, which was infiltrated with methylammonium lead iodide perovskite material.

Another study in the perovskite material system achieved a relative PCE enhancement of 15.7%.[126] A broadband absorption enhancement was demonstrated through the addition of Au−Ag alloy popcorn-shaped nanoparticles to the device. These nanoparticles were synthesized through a co-reduction of $HAuCl_4$ and $AgNO_3$ and had an average size of 150 ± 50 nm. The nanoparticles were embedded in the mesoporous TiO_2 at a concentration of 0.7 wt %.[126]

Higher efficiencies have been achieved in perovskite solar cells compared to OPV devices, and therefore these devices have less to gain from plasmonic enhancement schemes. The high efficiency is due to both substantial absorptivity near the band gap energy and superior charge transport. However, plasmonic enhancements could potentially enable materials savings even in high-efficiency systems.

Colloidal Quantum Dot Solar Cells. Several different device architectures have been employed to make high-performing CQD solar cells.[16,107,127−135] All consist of close-packed CQD films sandwiched between selective transparent and reflective contacts.[132] Like OPV devices, CQD cells must overcome an absorption−extraction compromise to reach high performance, and several plasmonic enhancement strategies have been deployed to address this compromise.

To enhance the absorption specifically in the infrared regime, a study[107] added 120 nm diameter core−15 nm shell SiO_2−Au core−shell nanoparticles to the active layer of a depleted heterojunction cell. In the lead sulfide (PbS) matrix, the nanoshells exhibit an LSPR peak at 820 nm. An enhancement in infrared photocurrent led to an 11% PCE improvement over a control device.[107]

Absorption enhancements in the active layer of a CQD solar cell have also been achieved by using the near-field enhancement associated with small (5 nm diameter) Au nanoparticles instead of focusing on far-field scattering gains.[134] The study demonstrated evidence of hot-electron transfer directly from the excited metal particles to the PbS semiconductor nanocrystals. The best-performing cell had a 12.5% PCE improvement over a nonplasmonic device.[134]

Plasmonic particles can play electronic as well as optical roles in CQD solar cells. One study built a Ag nanoparticle−PbS CQD nano-Schottky junction device by depositing self-assembled 40 nm diameter Ag hemispheres that covered 33% of the indium tin oxide (ITO) contact.[135] The PCE was enhanced by 58.1% compared to the fabricated control devices, which used a planar silver architecture. The improved performance was attributed to the modified absorption profile due to the enhanced optical field around the nanoparticles. This ensured that carriers were generated close to the metal−semiconductor interface within the depletion region.

Generally, plasmonically enhanced CQD devices have benefited from absorption improvements near the weakly absorbing quantum dot band gap edge. The overall PCE enhancements have generally been weakened by mild loss in V_{OC} and FF.

Summary. The largest relative improvements in all three materials systems were achieved in cells with low starting efficiencies and device absorption.[123,135] Incorporating plasmonic particles generally increased film absorption, although none of the plasmonically enhanced devices achieved record efficiencies in their respective classes nor approached the theoretical photocurrent limits based on the photovoltaic material band gaps. Addressing the question of whether the full parameter space has yet to be explored in these systems or if plasmonic enhancement schemes are fundamentally limited in practical devices remains an important research challenge.

PRACTICAL LIMITS OF PLASMONIC ENHANCEMENT

There are several practical obstacles to using plasmonic structures as photocurrent enhancers, which need to be taken into account for plasmonic solar cell design. The biggest barrier is the presence of parasitic absorption in the nanoparticles.[83,136−139] Parasitic absorption refers to the loss of photocarriers excited in the metal particles themselves that decay via nonradiative channels to produce heat. This process competes with useful absorption in the photovoltaic material. The relative amount of parasitic absorption versus useful near- and far-field scattering in the metal can be manipulated to some extent by controlling the size, morphology, material, and placement of the metallic nanoparticles.

Another practical limitation is that embedded plasmonic nanostructures can act as carrier recombination centers in the absorbing medium,[122,140,141] often leading to a reduction in device open-circuit voltage as well as current.[142] Including a small insulating barrier in the form of a ligand or dielectric shell around the plasmonic nanostructure can suppress this effect but can also reduce the evanescent spatial field overlap with the photovoltaic absorber, thereby limiting the potential for absorption enhancement.

Other practical issues that arise in plasmonic solar cell design include chemical and physical compatibility of the solvents associated with the plasmonic and photovoltaic materials, and materials costs of the precious metals employed as nanoparticles (primarily gold and silver). Finally, there is the issue of resulting spectral trade-offs. Plasmonic structures have the ability to enhance a spectral regime where there is incomplete absorption in the photovoltaic material. However, in regimes where absorption is substantially complete, introducing plasmonic structures has the potential to degrade the system.

DOI: 10.1021/acsphotonics.5b00428
ACS Photonics 2016, 3, 158−173

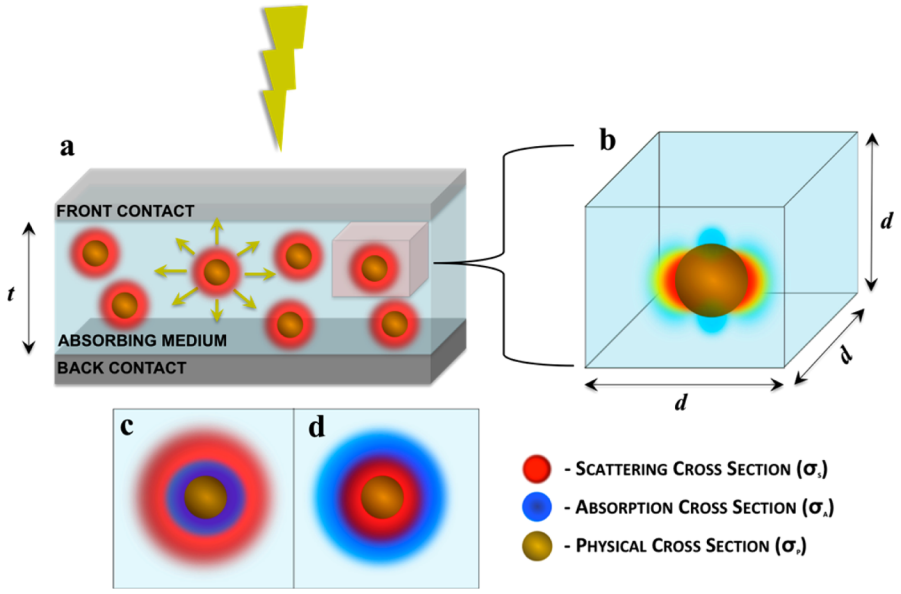

Figure 1. (a) Photovoltaic absorbing medium sandwiched between top and bottom contacts with randomly distributed embedded plasmonic nanoparticles. (b) Unit cube with side length d based on the average particle spacing used to evaluate the effect of a single plasmonic nanoparticle on the film. (c) Cross-section of the unit cell illustrating the case where the nanoparticle scattering cross-section exceeds the absorption cross-section. (d) Cross-section of the unit cell illustrating the case where the nanoparticle absorption cross-section exceeds the scattering cross-section.

Therefore, it is important to be tactical both in understanding the associated spectra[143,144] and in choosing the type, size, shape, and placement within the device of the plasmonic nanostructures.[145−147]

■ ABSORPTION ENHANCEMENT MODEL

Taking into account the practical enhancement limitations described above, it is clear that questions remain about the potential for using plasmonic nanoparticles as enhancers in real photovoltaic systems. Specifically, given a set of photovoltaic and plasmonic nanomaterials of interest, it would be useful to be able to quantitatively evaluate the potential photocurrent enhancement using an intuitive model that takes into account the experimental degrees of freedom present in the system. These parameters include the metal nanoparticle material, size, and shape; the thickness and identity of the photovoltaic active layer; and the relative concentration or number density of the embedded plasmonic particles. Adjusting and optimizing these factors experimentally is time- and materials-intensive, given the large parameter space.

We have developed an analytical model that can be used to evaluate the potential absorption enhancement in embedded plasmonic nanoparticle systems over a large parameter space. The results can be translated into potential photocurrent (J_{SC}) enhancement with the assumption of perfect carrier collection. The model determines the effective absorption coefficient and thickness of a photovoltaic film embedded with plasmonic nanoparticles based on the physical and optical properties of the constituent materials. These calculated effective parameters are, in turn, translated to an effective absorption, taking inspiration from effective medium approaches for estimating the optical properties of mixed media.

Effective medium approximations (EMAs), such as the Bruggeman model[148] and the Maxwell−Garnett theory (MGT),[149] treat a heterogeneous medium as one that is homogeneous by effectively averaging the properties of the individual constituent materials. In the MGT, the model medium is composed of spherical particles embedded in a host material. This theory assumes that the composite material is electrodynamically isotropic and possesses a linear response to incident light. Other assumptions include that the mixture parameters are static (nonparametric), the nanoparticle inclusions are separated by distances that surpass their individual sizes, and the sizes of the inclusions are small in comparison to the wavelength of light in the integrated medium. The Bruggeman model is an extension of the MGT that facilitates the inclusion of polydisperse particles.

Our proposed model is an intuitive extension and approximation of an effective medium theory for a specific system: plasmonically enhanced thin-film photovoltaics. The model makes similar assumptions to the MGT, including the isotropic nature of the materials and the monodispersity of the nanoparticle inclusions, but accounts for the plasmonic response by using simulated nanoparticle scattering and absorption cross-sections.

The model takes as inputs the absorption coefficient, α [m^{-1}], of the photovoltaic material; the photovoltaic film thickness, t [m], along the illumination direction; the physical cross-section, σ_p [m^2]; the scattering cross-section, σ_s [m^2]; and the absorption cross-section, σ_a [m^2], of the embedded plasmonic nanoparticles. The physical cross-section is usually defined as the 2D projection of the physical volume occupied by the nanoparticle. The absorption cross-section quantifies the rate at which energy is removed through absorption from an incident field, and the scattering cross-section quantifies the net power reflected from the nanoparticle. The scattering and absorption cross-sections can be calculated using Mie theory[150,151] or numerically via finite-difference time-domain (FDTD) simulations[152,153] or finite element methods[154,155] with the absorbing medium used as the background. Scattering and absorption efficiencies, Q_s and Q_a, are defined as the ratios of the scattering and absorption cross-sections, respectively, to the physical cross-section of the plasmonic nanoparticles ($Q_s = \sigma_s/\sigma_p$; $Q_a = \sigma_a/\sigma_p$). The absorption cross-section, scattering

DOI: 10.1021/acsphotonics.5b00428
ACS Photonics 2016, 3, 158−173

cross-section, absorption efficiency, scattering efficiency, and absorption coefficient are all wavelength-dependent in general.

Our model assumes that the nanoparticles are randomly and uniformly distributed within the photovoltaic film with an average number density. We use the concept of a unit cell to represent the concentration (number density), ρ [m^{-3}], of the nanoparticles within the absorbing medium. The unit cell is a cube with one nanoparticle at the center, such that the side length, d [m], is related to the concentration as

$$\rho = \frac{1}{d^3} \tag{1}$$

In addition, we define a unitless variable C to represent the relative separation between the nanoparticles:

$$C = \frac{d}{D} \tag{2}$$

where D is the diameter [m] (or length for nonspherical particles) of the nanoparticles.

Neglecting reflection at the photovoltaic absorber surface, we use the Beer–Lambert law[156] to calculate the absorption, A_1, in the unmodified photovoltaic film and the absorption, A_2, in the film with the embedded plasmonic particles:

$$A_1 = 1 - e^{-\alpha t} \tag{3}$$

$$A_2 = 1 - e^{-\alpha_{plasmonic} t_{plasmonic}} \tag{4}$$

$$\alpha_{plasmonic} = \alpha\left[1 + \frac{\sigma_p}{d^2}(Q_s - Q_a)\right] \tag{5}$$

$$t_{plasmonic} = t\sqrt{1 - \frac{\sigma_p}{d^2}} \tag{6}$$

Equations 5 and 6 relate the new effective absorption coefficient ($\alpha_{plasmonic}$) and the new effective film thickness ($t_{plasmonic}$), respectively, to the materials system parameters. In eq 5, $\alpha_{plasmonic}$ represents the effect that a single plasmonic nanoparticle has on the surrounding medium. The MGT uses a cubic lattice of nanoparticles in a medium to approximate the effective dielectric constant by accounting for the volume fraction taken up by the inclusions as well as the relative permittivities of the medium and inclusions. In a similar fashion, we use the plasmonic properties of a single nanoparticle and the optical properties of the medium to approximate the effective absorption coefficient. $\alpha_{plasmonic}$ can be larger or smaller than the absorption coefficient of the bare medium, depending on the relative values of the scattering, absorption, and physical cross-sections of the plasmonic nanoparticle inclusions, as well as the number density of the nanoparticles, represented by their average 2D spacing, d^2. The scattering cross-section effectively adds to the absorptivity of the medium, while the absorption cross-section effectively subtracts from the absorptivity of the medium. Also, the physical loss of absorbing medium caused by replacing a fraction of the material with nanoparticles is accounted for in eq 6, which subtracts the projection of the physical area occupied by the nanoparticles from the cross-section of the unit cell.

This model accounts for the parasitic absorption that takes place within the metal nanoparticles, which is a source of photocarrier loss, by subtracting a term proportional to Q_a in the expression for $\alpha_{plasmonic}$. It requires input from numerical electrodynamic simulations in the form of single-particle absorption and scattering cross-sections. The total-field scattered-field (TFSF) source method[157] in FDTD simulations yields an effective scattering cross-section that can account for both the near- and far-field scattering associated with the nanoparticle. Thus, both conventional far-field scattering and "local-field" effects are incorporated in the model.

Using eqs 3–6, we can define a quantitative figure of merit, M, which is a measure of the absorption enhancement in the photovoltaic system due to adding the embedded plasmonic nanostructures:

$$M = \frac{A_2}{A_1} - 1 \tag{7}$$

By integrating M over all wavelengths, the net absorption enhancement ($M_{total} > 0$) or loss ($M_{total} < 0$) factor can be calculated. Assuming perfect carrier collection (100% internal quantum efficiency, IQE), we can use this model to calculate the expected photocurrent enhancement in a photovoltaic device by integrating the product of the enhanced (A_2) or control absorptions (A_1), solar photon flux, and the elementary electric charge over all wavelengths.

This model requires only the calculation of the single-particle plasmonic optical properties as a prerequisite for estimating the properties of the bulk mixed media systems over a large range of parameters. This method is computationally fast compared to full numerical modeling of entire film structures with randomly embedded nanoparticles. In the following section, we will use the above model to make realistic predictions for achievable photocurrents in plasmonically enhanced photovoltaic devices and compare the results to previous experimental studies.

MODEL EVALUATION

Comparison to Experimental Studies. Previous demonstrations of embedded plasmonic nanoparticle enhancements in organic, hybrid organic–inorganic perovskite and colloidal quantum dot solar cells provide test systems for evaluating our model. We will examine one specific example from each of these three systems to analyze in detail: (1) Silver nanoclusters embedded in a poly [*N*-9″-heptadecanyl-2,7-carbazole-*alt*-5,5-(4′,7′-di-2-thienyl-2′,1′,3′-benzothiadiazole) (PCDTBT):[6,6]-phenyl C-71-butyric acid methyl ester ($PC_{70}BM$) mixture,[94] (2) Au/Ag alloy popcorn-shaped nanoparticles embedded in mesoporous TiO_2 and infiltrated with methylammonium lead iodide ($CH_3NH_3PbI_3$) perovskite,[126] and (3) SiO_2–Au core–shell nanospheres embedded in a PbS CQD thin film.[107] Absorption coefficients for the three photovoltaic materials were extracted from reported values in the literature.[107,158,159]

We employed FDTD simulations to calculate Q_s and Q_a for single plasmonic nanoparticles in the three examples using the total-field/scattered-field source method.[157,160−163] We used the average value of the real part of the refractive index of the three materials over a wavelength range of 300–800 nm for the PCDTBT:$PC_{70}BM$ mixture and $CH_3NH_3PbI_3$ perovskite material and 300–1200 nm for the PbS CQDs as the background in the simulations. The silver nanoclusters were represented by closely packed 40 nm diameter nanospheres with spacing extrapolated from Figure 3 of ref 67 and total diameter of 600 nm. The popcorn-shaped Au/Ag nanoparticles were modeled as nanospheres with diameters equal to the reported size of the alloyed particles (150 nm) and refractive indices given by the molar average of the refractive indices of

DOI: 10.1021/acsphotonics.5b00428
ACS Photonics 2016, 3, 158−173

Au and Ag based on the reported weight ratio.[126] The average real part of the refractive index of a PbS CQD film with the first exciton peak at 959 nm was used as the background for the 120 nm SiO_2 core/15 nm Au shell particles.[107]

Figure 2 shows that the relative scattering efficiency $(Q_s - Q_a)$ for all three types of plasmonic nanoparticles is positive over

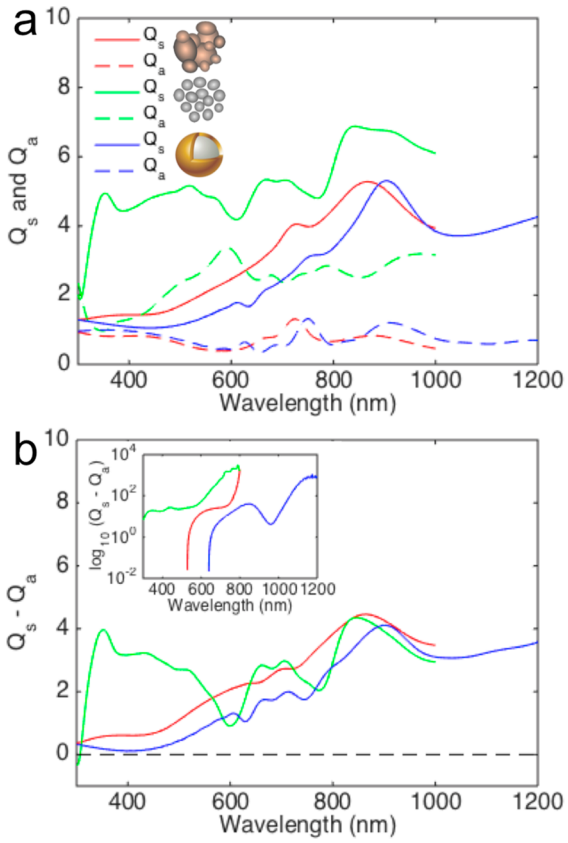

Figure 2. (a) Scattering efficiency (Q_s) and absorption efficiency (Q_a) vs wavelength for the three different plasmonic nanoparticle types calculated using single-particle FDTD simulations. Solid lines: Scattering efficiency. Dashed lines: Absorption efficiency. Red: 150 nm Au/Ag alloy popcorn nanoparticles embedded in a perovskite-infiltrated-TiO_2 background. Green: 40 nm silver nanoclusters embedded in a PCDTBT:$PC_{70}BM$ mixture. Blue: Nanoshells with 120 nm SiO_2 core and 15 nm Au shell thickness embedded in PbS CQD film background. (b) Relative scattering efficiency $(Q_s - Q_a)$ vs wavelength for the systems plotted in (a). Inset: Relative scattering efficiency $(Q_s - Q_a)$ required to achieve 90% absorption as a function of wavelength of the three systems at a relative nanoparticle separation $C = 3$.

most of the relevant wavelength ranges (the absorption of the organic and perovskite materials cuts off near 800 nm). Therefore, these three types of plasmonic nanoparticles are all predicted to be enhancers in their respective absorbing media. The inset in Figure 2b shows the relative scattering efficiencies required to achieve 90% absorption in the three systems at relative nanoparticle separations of $C = 3$. The fact that Q_s and Q_a are small compared to C in each study indicates that using single-particle simulations as the basis for calculating the optical properties of the system is a reasonable approximation. This validity condition can be written as

$$\max(\sqrt{Q_s}, \sqrt{Q_a}) < C \tag{8}$$

Equation 8 requires that there is no spatial overlap of the optical influences of adjacent nanoparticles.

The number density of the embedded plasmonic particles is an important experimental free parameter. There is an inherent trade-off in an embedded nanoparticle system: increasing the nanoparticle concentration can yield more scattering enhancement of the absorption in the photovoltaic material; however, the nanoparticles occupy physical volume that subtracts from the ability of the photovoltaic material to absorb light. Our model can be used to calculate the optimum nanoparticle density for each of the three test systems given the photovoltaic film thicknesses used in each case (80 nm for the PCDTBT:$PC_{70}BM$ film; 200 nm as an approximation of the average optical thickness of the perovskite-infiltrated-TiO_2 film; and 400 nm for the PbS CQD film).

Figure 3a is a plot of the predicted photocurrent and photocurrent enhancement as a function of relative nano-

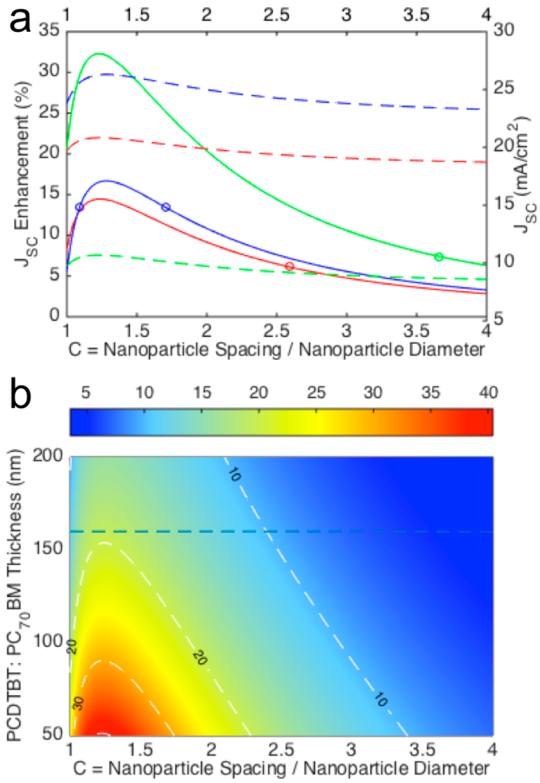

Figure 3. (a) Solid lines: Predicted J_{SC} enhancement (%) vs relative nanoparticle separation. The circles are experimental J_{SC} enhancement for the best-performing cells in each study. Dashed lines: Predicted J_{SC} values (mA/cm^2) vs relative nanoparticle separation. Red: 150 nm Au/Ag alloy popcorn embedded in perovskite-infiltrated TiO_2. Green: 40 nm silver nanoclusters embedded in PCDTBT:$PC_{70}BM$. Blue: 120 nm SiO_2 core/15 nm Au shell nanospheres in PbS CQD film. (b) Percent J_{SC} enhancement (color scale) as a function of film thickness and nanoparticle separation. The white dashed lines are contours at 10%, 20%, 30%, and 40% J_{SC} enhancement to guide the eye. The blue line indicates a thickness of 160 nm, twice the reported thickness in ref 67.

particle separation. There is an optimum separation, or number density, of embedded plasmonic nanoparticles in each case, and the predicted J_{SC} enhancement has a long tail extending to the limit of large nanoparticle separation. The circles correspond to the J_{SC} enhancement for the best-performing cells in each study, and estimated experimental values of C for the three

DOI: 10.1021/acsphotonics.5b00428
ACS Photonics 2016, 3, 158−173

systems were approximately 2−5, which lie in the large-separation/low-density range.[94,107,126] Generally, due to the difficulty in achieving precise control of the synthetic and deposition processes, there are multiple sources of error in the estimations of nanoparticle size and density; however, all experimentally observed enhancements fell within the range predicted by our model.

The largest relative photocurrent enhancements are predicted for the system composed of Ag nanoclusters embedded in PCDTBT:$PC_{70}BM$. This is primarily due to the small thickness (80 nm) of the absorbing film; intuitively, larger relative enhancements should be possible for thinner active layers in which initial absorption is less complete. We examined the effect of the thickness of the PCDTBT:$PC_{70}BM$ layer by varying it simultaneously with the effective nanoparticle separation to determine the potential J_{SC} enhancement as shown in Figure 3b. The maximum J_{SC} enhancement requires a thickness-independent high density of embedded plasmonic nanoparticles. The blue dashed line indicates a thickness of 160 nm, which is double the reported thickness in ref 67. If the organic layer thickness could be doubled, the predicted J_{SC} enhancement in the organic system is very close to that predicted in the other two systems. This reinforces the idea that plasmonic enhancements are potentially more useful in extremely thin films, even independent of photovoltaic material type, and that OPV cells in particular may have more to gain from embedded plasmonic enhancement schemes.

Effect of Nanoparticle Shape. Since our model uses calculated plasmonic absorption and scattering cross-sections as inputs, it can incorporate nonspherical nanoparticles, many of which have been used in embedded photovoltaic enhancement schemes.[93,124] Shape plays an important role in plasmonic nanoparticle properties.[145,164,164,165,165−171] Sharp edges can drastically increase local-field intensity while simultaneously introducing strong parasitic absorption.[165,166,168−170] We applied our model to systems composed of octahedral and truncated octahedral Au nanoparticles (70 nm in length) embedded in PCDTBT:$PC_{70}BM$[93] and compared them to a system with similarly sized Au nanospheres as the plasmonic material in the same matrix. The simulation results are shown in Figure 4.

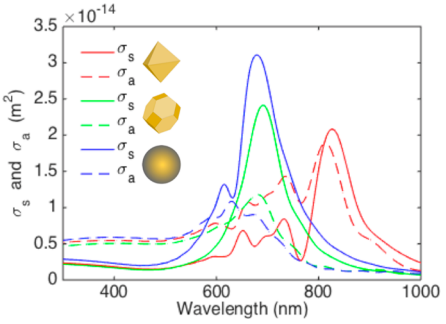

Figure 4. Scattering (solid lines) and absorption (dashed lines) cross-section vs wavelength for different shaped plasmonic nanoparticles of similar size embedded in a PCDTBT:$PC_{70}BM$ background. Red: 70 nm octahedral Au nanoparticles. Green: 70 nm truncated octahedral Au nanoparticles. Blue: 70 nm Au nanospheres.

The octahedral particles contain sharp points, while the truncated octahedra are much closer to spherical in shape. FDTD simulations indicate that gold nanospheres and truncated octahedra of similar size have similar optical properties. The truncated octahedra exhibit a slight red shift and a decrease of the scattering cross-section peak amplitude compared to the nanospheres. The regular octahedral nanoparticles exhibit smaller scattering amplitudes and an increase in absorption with a large red shift compared to the other particles. The absorption cross-section exceeds the scattering cross-section in the 300−800 nm spectral range, indicating that this particle type will not enhance absorption in a PCDTBT:$PC_{70}BM$ film.

Both the truncated octahedra and the nanospheres have scattering cross-sections larger than their absorption cross-sections near 700 nm in wavelength, indicating that both nanoparticle types have the potential to enhance photovoltaic absorption in this spectral range. However, at wavelengths shorter than 600 nm, the absorption cross-sections are generally larger than the scattering cross-sections, meaning that parasitic absorption will exceed any useful scattering enhancement in this range. This test case illustrates the need to engineer nanoparticle shape for a specific application and, generally, that shapes with sharp corners often introduce more parasitic absorption than useful scattering enhancements.

Effect of Nanoparticle Size and Material. The size dependence of the scattering and absorption properties of plasmonic nanoparticles is another useful tuning knob for optoelectronic applications.[170,172−174] We studied the size-dependent behavior of systems composed of Au and Ag nanospheres embedded in PCDTBT:$PC_{70}BM$. The results are shown in Figure 5. We used a fixed nanoparticle separation of $C = 2$ and a photovoltaic layer thickness of $t = 80$ nm for these calculations.

The relative scattering efficiency and the absorption enhancement red-shift as a function of nanoparticle size, as can be seen in Figure 5. The Au system exhibits significant parasitic absorption in the shorter wavelength regime. Figure 5c demonstrates that embedding these types of particles in the OPV film is predicted to result in no net J_{SC} enhancement. This is because parasitic absorption is predicted to dominate within the AM1.5G peak power range and relevant absorption window for PCDTBT:$PC_{70}BM$ of 300−800 nm.

One potential method for avoiding nanoparticle parasitic absorption in the strongly absorbing spectral ranges of the photovoltaic material is to embed nanoparticles at selective locations along the illumination direction of a device. Au nanoparticles such as those modeled in Figure 5 could be embedded at the back of a PCDTBT:$PC_{70}BM$ layer (farther from the illumination plane) so that shorter wavelength photons can be substantially absorbed before reaching the nanoparticle locations within the film. Only photons with wavelengths in the more weakly absorbing spectral region of PCDTBT:$PC_{70}BM$ and the more strongly scattering spectral region of the nanoparticles (600−800 nm) would have a high probability of interacting with the plasmonic elements, thereby enhancing total absorption in the device.

The system composed of Ag nanospheres embedded in PCDTBT:$PC_{70}BM$ behaves both qualitatively and quantitatively differently from the Au nanosphere system. As can be seen in Figure 5d, Ag nanospheres with diameters larger than 35 nm can be strong enhancers in PCDTBT:$PC_{70}BM$ at wavelengths near 650 nm. The spectral range of enhancement displays a red shift with increasing nanoparticle size. The main spectral peak corresponds to the dipole LSPR mode of the Ag nanospheres, and the overall enhancement is a result of competition between the scattering and parasitic absorption.

DOI: 10.1021/acsphotonics.5b00428
ACS Photonics 2016, 3, 158−173

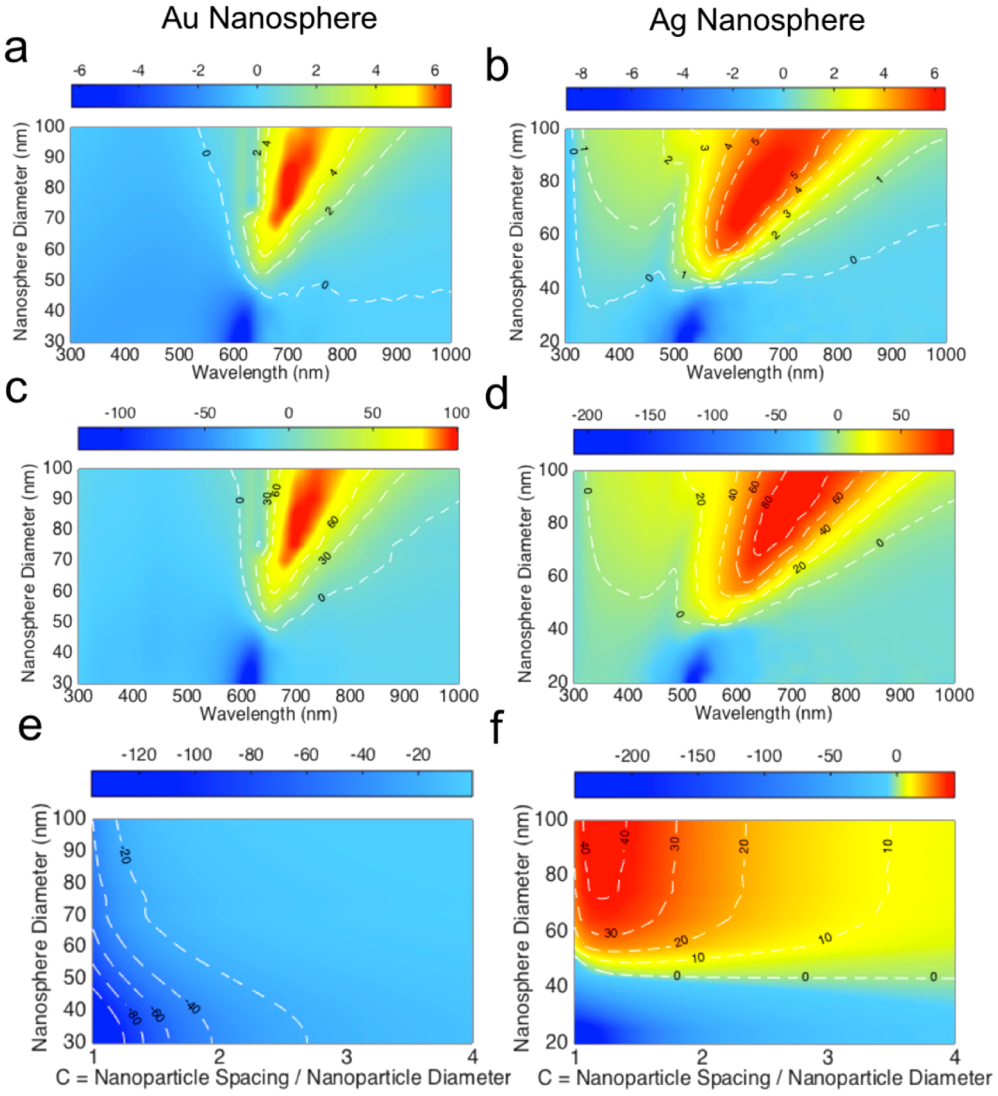

Figure 5. (a, b) Relative scattering efficiency ($Q_s - Q_a$) vs wavelength and particle size for Au (a) and Ag (b) nanospheres embedded in an organic film. The dashed contour lines represent $Q_s - Q_a$ as labeled. (c, d) Percent absorption enhancement or loss vs wavelength and particle size for Au (c) and Ag (d) nanospheres embedded in an organic film. The dashed contour lines represent relative percentage changes as labeled. (e, f) Percent J_{SC} loss or enhancement vs relative particle separation and particle size for Au (e) and Ag (f) nanospheres embedded in an organic film. The dashed contour lines represent relative percentage changes as labeled.

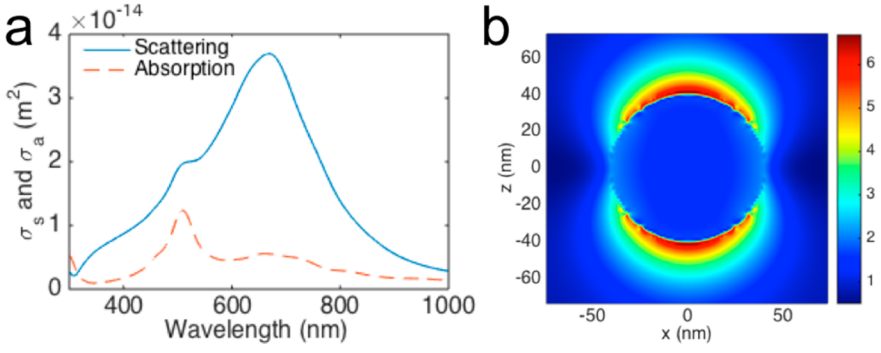

Figure 6. (a) Scattering and absorption cross-section vs wavelength for an 80 nm diameter Ag nanosphere embedded in a PCDTBT:$PC_{70}BM$ background. (b) Calculated normalized electric field intensity (λ = 680 nm) for a single Ag nanosphere at the plane normal to the incident illumination.

The calculated electric field profile of the LSPR mode at 680 nm and scattering and absorption cross-sections vs wavelength for an 80 nm diameter Ag nanosphere embedded in a PCDTBT:$PC_{70}BM$ film can be seen in Figure 6.

DOI: 10.1021/acsphotonics.5b00428
ACS Photonics 2016, 3, 158−173

Figure 5e shows the wavelength-dependent absorption enhancement for different sized Ag nanospheres. Due to the high absorptivity of PCDTBT:$PC_{70}BM$ below 500 nm, most of the light in this range is absorbed in 80 nm of material without the integration of plasmonic nanoparticles. Since the absorptivity of PCDTBT:$PC_{70}BM$ between 600 and 800 nm is low, exploiting nanoparticles with strong scattering in this spectral range results in an absorption enhancement, with the peak enhancement exhibiting a red shift as a function of nanoparticle size.

Using the AM1.5G spectrum as our input, we calculated the predicted J_{SC} enhancement as a function of Ag nanosphere size and number density. The results are shown in Figure 5f; significant J_{SC} enhancements can be achieved for Ag nanospheres with diameters larger than 45 nm. Larger Ag nanospheres and higher number densities result in larger predicted J_{SC} enhancements. For all sizes of embedded Ag nanospheres, the predicted J_{SC} enhancement has a long and relatively flat tail in the large nanoparticle separation limit and becomes very sensitive to separation changes in the high number density limit.

Model Validity. The above model estimates the effective absorption in an absorbing photovoltaic layer using the Beer−Lambert law, which describes bulk absorption in a homogeneous medium. However, in a typical multilayer solution-processed thin-film solar cell, the layer thicknesses are on the scale of the wavelengths of interest, and, as a result, interference effects can play an influential role in real device absorption. These interference effects could be included in our model by embedding the expression for absorption within a thin-film interference calculation framework such as the transfer matrix method (TMM) for a multilayered structure.[175] Such methods take as inputs the thicknesses and the wavelength-dependent complex indices of refraction of the different optical material layers. Our model predicts the new effective absorption coefficient of the modified absorbing medium in a system containing embedded plasmonic nanoparticles. This absorption coefficient is directly related to the imaginary part of the refractive index function; however, estimating an effective real part is more complicated due to the surface plasmon condition that the real part of the dielectric function changes signs across an interface.

In order to test the effect of thin-film interference on the sample device absorption results described above, we input the modified imaginary part of the refractive index from our model into a TMM solver[176] and varied the real part by using small perturbations around the original values for a given set of CQD device layer thicknesses.[107] The main effect on total device absorption was due to the addition of a back reflective contact and was less sensitive to variations in the thickness of the front illuminated side transparent contact layers. Due to interference effects, the predicted photocurrents calculated using the TMM were slightly higher (by less than 10%) than the predictions using the Beer−Lambert-based model above, but the overarching trends associated with relative nanoparticle concentration were preserved. A ±10% perturbation of the real part of the refractive index of the active layer resulted in a ±8% shift in the original predicted photocurrents.

Although calculations that take thin-film interference effects into account must be used to make accurate predictions of the photocurrent in a real device structure, our enhancement model can be used to evaluate the total absorption enhancement potential associated with an embedded plasmonic nanoparticle strategy as a function of particle type, size, and concentration. Specific device designs can then be fine-tuned by using thin-film interference and other light-trapping effects.

As previously mentioned, the model described above is a good approximation for real systems when eq 8 is satisfied, i.e., when the average nanoparticle concentration is relatively small. This is borne out by the close match of the predicted J_{SC} enhancements with the reported experimental results. When eq 8 is not satisfied, the model can still be used, but coupling effects between the nanoparticles must be taken into account via simulation of the optical properties of a larger system.[173,174] In addition, at higher nanoparticle concentrations, our model becomes less accurate due to strong nanoparticle scattering effects and the breakdown of the plane-wave condition for the Beer−Lambert law.

The model predicts absorption enhancement and corresponding J_{SC} enhancement by assuming perfect carrier collection (IQE) in the photovoltaic systems. However, it is possible to include carrier loss induced by the nanoparticle inclusions into the model, and models that account for both optical and electrical effects have been developed for other proposed systems.[177−180] This could be achieved, for example, by calculating the effective nanoparticle electronic trap capture cross-section and subtracting the trapping efficiency from the Q terms in the calculation of $\alpha_{plasmonic}$ (eq 5). Other carrier loss mechanisms in real devices could be included through experimental IQE measurements.

PERSPECTIVE AND FUTURE DIRECTIONS FOR SOLUTION-PROCESSED SOLAR CELLS

General strategies for designing an effective plasmonic enhancement scheme for a specific photovoltaic system can be based on the following two steps:

1. Choose an appropriate material, shape, and size in which the scattering cross-section is larger than the absorption cross-section within the photovoltaic material of interest for the intended spectral enhancement range.
2. An effective medium approach, such as the model described here, can be used to select the optimum embedded nanoparticle density for maximum plasmonic absorption enhancement of the photovoltaic medium.

As has been demonstrated through successful experiments, this strategy can lead to absorption and consequent photocurrent enhancements in real devices. Careful analysis of the model described above, however, indicates that the absolute magnitude of the potential enhancements may be limited. Specifically, in CQD and perovskite solar cells, the model predicts that the maximum achievable plasmonic photocurrent enhancements can probably improve upon the current best-performing devices by only about 15%, corresponding to 1−4 mA/cm^2 of additional photocurrent. Given these results and the history of steady transport improvements in these materials, we recommend that the fields concentrate instead on improving fundamental materials properties such as decreasing electronic trap state densities and increasing charge carrier diffusion lengths through improved passivation and growth methods. Plasmonic enhancements are of most interest for applications where external considerations limit the thickness of the active material to less than that already utilized in the best-performing devices.

In contrast, the outlook for plasmonic enhancements in organic photovoltaics may be much brighter. Active layer thicknesses are

DOI: 10.1021/acsphotonics.5b00428
ACS Photonics 2016, 3, 158−173

smaller in the best-performing OPV classes due to limitations on exciton dissociation and diffusion. Therefore, plasmonic photocurrent enhancements of up to 40% are predicted by our model, as can be seen in Figure 5. Specifically, the field should concentrate on using large (up to 100 nm) silver particles for OPV films due to the LSPR spectral overlap and reduced parasitic absorption at shorter wavelengths, and nanoparticle shapes with pointed vertices should be avoided due to the parasitic absorption induced by the sharp edges. From a practical standpoint, care must be taken in using large nanoparticles for thin-film enhancement to avoid the formation of detrimental shunt paths in devices. Critically, further absorption and photocurrent enhancements are predicted to be possible at larger embedded nanoparticle densities than have previously been explored. However, the density must be fine-tuned in order to achieve optimum performance due to the sharply peaked nature of the predicted enhancement curves, as seen in Figure 3. In recent years, there have been improvements in achieving thicker absorbing layers for OPVs,[181] and the maturation of these improvements would render plasmonic enhancements less applicable.

In addition to emphasizing work on plasmonically enhanced OPV, we propose two relatively unexplored plasmonic enhancement paths. The first is aggressively pursuing new plasmonic materials strategies. Gold and silver have been the most commonly used plasmonic materials in photovoltaics due to their low-loss behavior in the visible wavelength range resulting from the relatively small values of the imaginary parts of the dielectric function. Alternatives such as aluminum, copper, and indium tin oxide also have the potential for low loss in specific spectral ranges. New strategies that take advantage of these materials could include spatially integrating ITO nanoparticles at the base of a tandem device to enhance infrared absorption or using aluminum nanoparticles for ultraviolet absorption enhancement in thin absorbing active layers. Additionally, alloying different metals to achieve "averaging" of the spectral properties for broadband enhancement is an attractive potential strategy.

The second path of interest is pursuing electronic coupling to make true hybrid plasmonic-excitonic materials. Instead of considering only the optical properties of plasmonic enhancers in forming an effective medium, full treatment of the electronic effects of these materials could make plasmonic materials of interest for multiple classes of solution-processed solar cells. The goal would be to use coherent electronic coupling of plasmonic particles to semiconducting media in order to engineer the excitonic structure. This material hybridization strategy could be used to extend the spectral sensitivity of organic materials to infrared wavelengths, for example, or could be used to modify the band structure CQD films to increase absorption near the exciton wavelengths while aiding in transport.

In conclusion, as the field of plasmonically enhanced solar cells matures, focusing on strategies with the highest potential for enabling real performance advances is of increasing interest. We believe this entails adjusting nanoparticle concentration as the most crucial tuning knob in embedded plasmonically enhanced photovoltaic devices, working on the specific silver-based strategy outlined for OPV and pursuing the advanced methods described above that go beyond the traditional gold/silver optical enhancement paradigm.

AUTHOR INFORMATION

Corresponding Author

*E-mail: susanna.thon@jhu.edu.

Notes

The authors declare no competing financial interest.

ACKNOWLEDGMENTS

The authors would like to thank Y. Cheng, N. Palmquist, and G. Qian for useful discussions and technical assistance over the course of this study.

REFERENCES

(1) Günes, S.; Neugebauer, H.; Sariciftci, N. S. Conjugated Polymer-Based Organic Solar Cells. *Chem. Rev.* **2007**, *107*, 1324−1338.

(2) Shaheen, S. E.; Brabec, C. J.; Sariciftci, N. S.; Padinger, F.; Fromherz, T.; Hummelen, J. C. 2.5% Efficient Organic Plastic Solar Cells. *Appl. Phys. Lett.* **2001**, *78*, 841−843.

(3) Rowell, M. W.; Topinka, M. A.; McGehee, M. D.; Prall, H.-J.; Dennler, G.; Sariciftci, N. S.; Hu, L.; Gruner, G. Organic Solar Cells with Carbon Nanotube Network Electrodes. *Appl. Phys. Lett.* **2006**, *88*, 233506.

(4) Clarke, T. M.; Durrant, J. R. Charge Photogeneration in Organic Solar Cells. *Chem. Rev.* **2010**, *110*, 6736−6767.

(5) Brédas, J.-L.; Norton, J. E.; Cornil, J.; Coropceanu, V. Molecular Understanding of Organic Solar Cells: The Challenges. *Acc. Chem. Res.* **2009**, *42*, 1691−1699.

(6) Liu, M.; Johnston, M. B.; Snaith, H. J. Efficient Planar Heterojunction Perovskite Solar Cells by Vapour Deposition. *Nature* **2013**, *501*, 395−398.

(7) Ball, J. M.; Lee, M. M.; Hey, A.; Snaith, H. J. Low-Temperature Processed Meso-Superstructured to Thin-Film Perovskite Solar Cells. *Energy Environ. Sci.* **2013**, *6*, 1739−1743.

(8) Zhou, H.; Chen, Q.; Li, G.; Luo, S.; Song, T.; Duan, H.-S.; Hong, Z.; You, J.; Liu, Y.; Yang, Y. Interface Engineering of Highly Efficient Perovskite Solar Cells. *Science* **2014**, *345*, 542−546.

(9) Liu, D.; Kelly, T. L. Perovskite Solar Cells with a Planar Heterojunction Structure Prepared Using Room-Temperature Solution Processing Techniques. *Nat. Photonics* **2014**, *8*, 133−138.

(10) Green, M. A.; Ho-Baillie, A.; Snaith, H. J. The Emergence of Perovskite Solar Cells. *Nat. Photonics* **2014**, *8*, 506−514.

(11) Kamat, P. V. Quantum Dot Solar Cells. Semiconductor Nanocrystals as Light Harvesters†. *J. Phys. Chem. C* **2008**, *112*, 18737−18753.

(12) Kramer, I. J.; Sargent, E. H. Colloidal Quantum Dot Photovoltaics: A Path Forward. *ACS Nano* **2011**, *5*, 8506−8514.

(13) Pattantyus-Abraham, A. G.; Kramer, I. J.; Barkhouse, A. R.; Wang, X.; Konstantatos, G.; Debnath, R.; Levina, L.; Raabe, I.; Nazeeruddin, M. K.; Grätzel, M.; Sargent, E. H. Depleted-Heterojunction Colloidal Quantum Dot Solar Cells. *ACS Nano* **2010**, *4*, 3374−3380.

(14) Ip, A. H.; Thon, S. M.; Hoogland, S.; Voznyy, O.; Zhitomirsky, D.; Debnath, R.; Levina, L.; Rollny, L. R.; Carey, G. H.; Fischer, A.; Kemp, K. W.; Kramer, I. J.; Ning, Z.; Labelle, A. J.; Chou, K. W.; Amassian, A.; Sargent, E. H. Hybrid Passivated Colloidal Quantum Dot Solids. *Nat. Nanotechnol.* **2012**, *7*, 577−582.

(15) Koleilat, G. I.; Levina, L.; Shukla, H.; Myrskog, S. H.; Hinds, S.; Pattantyus-Abraham, A. G.; Sargent, E. H. Efficient, Stable Infrared Photovoltaics Based on Solution-Cast Colloidal Quantum Dots. *ACS Nano* **2008**, *2*, 833−840.

(16) Tang, J.; Kemp, K. W.; Hoogland, S.; Jeong, K. S.; Liu, H.; Levina, L.; Furukawa, M.; Wang, X.; Debnath, R.; Cha, D.; Chou, K. W.; Fischer, A.; Amassian, A.; Asbury, J. B.; Sargent, E. H. Colloidal-Quantum-Dot Photovoltaics Using Atomic-Ligand Passivation. *Nat. Mater.* **2011**, *10*, 765−771.

(17) Park, S. H.; Roy, A.; Beaupré, S.; Cho, S.; Coates, N.; Moon, J. S.; Moses, D.; Leclerc, M.; Lee, K.; Heeger, A. J. Bulk Heterojunction

DOI: 10.1021/acsphotonics.5b00428
ACS Photonics 2016, 3, 158−173

Solar Cells with Internal Quantum Efficiency Approaching 100%. *Nat. Photonics* **2009**, *3*, 297−302.
(18) Liang, Y.; Feng, D.; Wu, Y.; Tsai, S.-T.; Li, G.; Ray, C.; Yu, L. Highly Efficient Solar Cell Polymers Developed via Fine-Tuning of Structural and Electronic Properties. *J. Am. Chem. Soc.* **2009**, *131*, 7792−7799.
(19) Lee, M. M.; Teuscher, J.; Miyasaka, T.; Murakami, T. N.; Snaith, H. J. Efficient Hybrid Solar Cells Based on Meso-Superstructured Organometal Halide Perovskites. *Science* **2012**, *338*, 643−647.
(20) Barkhouse, D. A. R.; Pattantyus-Abraham, A. G.; Levina, L.; Sargent, E. H. Thiols Passivate Recombination Centers in Colloidal Quantum Dots Leading to Enhanced Photovoltaic Device Efficiency. *ACS Nano* **2008**, *2*, 2356−2362.
(21) Heremans, P.; Cheyns, D.; Rand, B. P. Strategies for Increasing the Efficiency of Heterojunction Organic Solar Cells: Material Selection and Device Architecture. *Acc. Chem. Res.* **2009**, *42*, 1740−1747.
(22) Kim, J. Y.; Kim, S. H.; Lee, H.-H.; Lee, K.; Ma, W.; Gong, X.; Heeger, A. J. New Architecture for High-Efficiency Polymer Photovoltaic Cells Using Solution-Based Titanium Oxide as an Optical Spacer. *Adv. Mater.* **2006**, *18*, 572−576.
(23) Kramer, I. J.; Sargent, E. H. The Architecture of Colloidal Quantum Dot Solar Cells: Materials to Devices. *Chem. Rev.* **2014**, *114*, 863−882.
(24) Im, J.-H.; Lee, C.-R.; Lee, J.-W.; Park, S.-W.; Park, N.-G. 6.5% Efficient Perovskite Quantum-Dot-Sensitized Solar Cell. *Nanoscale* **2011**, *3*, 4088−4093.
(25) Heo, J. H.; Im, S. H.; Noh, J. H.; Mandal, T. N.; Lim, C.-S.; Chang, J. A.; Lee, Y. H.; Kim, H.; Sarkar, A.; Nazeeruddin, M. K.; Grätzel, M.; Seok, S. I. Efficient Inorganic-Organic Hybrid Heterojunction Solar Cells Containing Perovskite Compound and Polymeric Hole Conductors. *Nat. Photonics* **2013**, *7*, 486−491.
(26) Dabirian, A.; Taghavinia, N. Theoretical Study of Light Trapping in Nanostructured Thin Film Solar Cells Using Wavelength-Scale Silver Particles. *ACS Appl. Mater. Interfaces* **2015**, *7*, 14926.
(27) Niggemann, M.; Riede, M.; Gombert, A.; Leo, K. Light Trapping in Organic Solar Cells. *Phys. Status Solidi A* **2008**, *205*, 2862−2874.
(28) Rim, S.-B.; Zhao, S.; Scully, S. R.; McGehee, M. D.; Peumans, P. An Effective Light Trapping Configuration for Thin-Film Solar Cells. *Appl. Phys. Lett.* **2007**, *91*, 243501.
(29) Polman, A.; Atwater, H. A. Photonic Design Principles for Ultrahigh-Efficiency Photovoltaics. *Nat. Mater.* **2012**, *11*, 174−177.
(30) Chou, C.-H.; Chen, F.-C. Plasmonic Nanostructures for Light Trapping in Organic Photovoltaic Devices. *Nanoscale* **2014**, *6*, 8444.
(31) Zhang, W.; Saliba, M.; Stranks, S. D.; Sun, Y.; Shi, X.; Wiesner, U.; Snaith, H. J. Enhancement of Perovskite-Based Solar Cells Employing Core−Shell Metal Nanoparticles. *Nano Lett.* **2013**, *13*, 4505−4510.
(32) Atwater, H. A. The Promise of Plasmonics. *Sci. Am.* **2007**, *296*, 56−62.
(33) Gramotnev, D. K.; Bozhevolnyi, S. I. Plasmonics beyond the Diffraction Limit. *Nat. Photonics* **2010**, *4*, 83−91.
(34) Schuller, J. A.; Barnard, E. S.; Cai, W.; Jun, Y. C.; White, J. S.; Brongersma, M. L. Plasmonics for Extreme Light Concentration and Manipulation. *Nat. Mater.* **2010**, *9*, 193−204.
(35) Maier, S. A.; Atwater, H. A. Plasmonics: Localization and Guiding of Electromagnetic Energy in Metal/dielectric Structures. *J. Appl. Phys.* **2005**, *98*, 011101.
(36) Ozbay, E. Plasmonics: Merging Photonics and Electronics at Nanoscale Dimensions. *Science* **2006**, *311*, 189−193.
(37) Maier, S. A. *Plasmonics: Fundamentals and Applications*; Springer Science & Business Media, 2007.
(38) Tang, C. W. Two-layer Organic Photovoltaic Cell. *Appl. Phys. Lett.* **1986**, *48*, 183−185.
(39) Luhman, W. A.; Holmes, R. J. Investigation of Energy Transfer in Organic Photovoltaic Cells and Impact on Exciton Diffusion Length Measurements. *Adv. Funct. Mater.* **2011**, *21*, 764−771.
(40) Mikhnenko, O. V.; Azimi, H.; Scharber, M.; Morana, M.; Blom, P. W. M.; Loi, M. A. Exciton Diffusion Length in Narrow Bandgap Polymers. *Energy Environ. Sci.* **2012**, *5*, 6960−6965.
(41) Stübinger, T.; Brütting, W. Exciton Diffusion and Optical Interference in Organic Donor−acceptor Photovoltaic Cells. *J. Appl. Phys.* **2001**, *90*, 3632−3641.
(42) Lunt, R. R.; Giebink, N. C.; Belak, A. A.; Benziger, J. B.; Forrest, S. R. Exciton Diffusion Lengths of Organic Semiconductor Thin Films Measured by Spectrally Resolved Photoluminescence Quenching. *J. Appl. Phys.* **2009**, *105*, 053711.
(43) Shaw, P. E.; Ruseckas, A.; Samuel, I. D. W. Exciton Diffusion Measurements in Poly(3-Hexylthiophene). *Adv. Mater.* **2008**, *20*, 3516−3520.
(44) Hiramoto, M.; Fujiwara, H.; Yokoyama, M. P-i-n like Behavior in Three-layered Organic Solar Cells Having a Co-deposited Interlayer of Pigments. *J. Appl. Phys.* **1992**, *72*, 3781−3787.
(45) Halls, J. J. M.; Walsh, C. A.; Greenham, N. C.; Marseglia, E. A.; Friend, R. H.; Moratti, S. C.; Holmes, A. B. Efficient Photodiodes from Interpenetrating Polymer Networks. *Nature* **1995**, *376*, 498−500.
(46) Peet, J.; Soci, C.; Coffin, R. C.; Nguyen, T. Q.; Mikhailovsky, A.; Moses, D.; Bazan, G. C. Method for Increasing the Photoconductive Response in Conjugated Polymer/fullerene Composites. *Appl. Phys. Lett.* **2006**, *89*, 252105.
(47) Peet, J.; Kim, J. Y.; Coates, N. E.; Ma, W. L.; Moses, D.; Heeger, A. J.; Bazan, G. C. Efficiency Enhancement in Low-Bandgap Polymer Solar Cells by Processing with Alkane Dithiols. *Nat. Mater.* **2007**, *6*, 497−500.
(48) Chen, W.; Nikiforov, M. P.; Darling, S. B. Morphology Characterization in Organic and Hybrid Solar Cells. *Energy Environ. Sci.* **2012**, *5*, 8045−8074.
(49) Pattantyus-Abraham, A. G.; Kramer, I. J.; Barkhouse, A. R.; Wang, X.; Konstantatos, G.; Debnath, R.; Levina, L.; Raabe, I.; Nazeeruddin, M. K.; Grätzel, M.; Sargent, E. H. Depleted-Heterojunction Colloidal Quantum Dot Solar Cells. *ACS Nano* **2010**, *4*, 3374−3380.
(50) Tang, J.; Liu, H.; Zhitomirsky, D.; Hoogland, S.; Wang, X.; Furukawa, M.; Levina, L.; Sargent, E. H. Quantum Junction Solar Cells. *Nano Lett.* **2012**, *12*, 4889−4894.
(51) Chuang, C.-H. M.; Brown, P. R.; Bulović, V.; Bawendi, M. G. Improved Performance and Stability in Quantum Dot Solar Cells through Band Alignment Engineering. *Nat. Mater.* **2014**, *13*, 796−801.
(52) Barkhouse, D. A. R.; Debnath, R.; Kramer, I. J.; Zhitomirsky, D.; Pattantyus-Abraham, A. G.; Levina, L.; Etgar, L.; Grätzel, M.; Sargent, E. H. Depleted Bulk Heterojunction Colloidal Quantum Dot Photovoltaics. *Adv. Mater.* **2011**, *23*, 3134−3138.
(53) Zhitomirsky, D.; Voznyy, O.; Levina, L.; Hoogland, S.; Kemp, K. W.; Ip, A. H.; Thon, S. M.; Sargent, E. H. Engineering Colloidal Quantum Dot Solids within and beyond the Mobility-Invariant Regime. *Nat. Commun.* **2014**, *5*.10.1038/ncomms4803
(54) Kim, H.-S.; Lee, C.-R.; Im, J.-H.; Lee, K.-B.; Moehl, T.; Marchioro, A.; Moon, S.-J.; Humphry-Baker, R.; Yum, J.-H.; Moser, J. E.; Grätzel, M.; Park, N.-G. Lead Iodide Perovskite Sensitized All-Solid-State Submicron Thin Film Mesoscopic Solar Cell with Efficiency Exceeding 9%. *Sci. Rep.* **2012**, *2*.10.1038/srep00591
(55) Bi, D.; Moon, S.-J.; Häggman, L.; Boschloo, G.; Yang, L.; Johansson, E. M. J.; Nazeeruddin, M. K.; Grätzel, M.; Hagfeldt, A. Using a Two-Step Deposition Technique to Prepare Perovskite (CH3NH3PbI3) for Thin Film Solar Cells Based on ZrO2 and TiO2Mesostructures. *RSC Adv.* **2013**, *3*, 18762−18766.
(56) Noh, J. H.; Im, S. H.; Heo, J. H.; Mandal, T. N.; Seok, S. I. Chemical Management for Colorful, Efficient, and Stable Inorganic−Organic Hybrid Nanostructured Solar Cells. *Nano Lett.* **2013**, *13*, 1764−1769.
(57) Etgar, L.; Gao, P.; Xue, Z.; Peng, Q.; Chandiran, A. K.; Liu, B.; Nazeeruddin, M. K.; Grätzel, M. Mesoscopic CH3NH3PbI3/TiO2 Heterojunction Solar Cells. *J. Am. Chem. Soc.* **2012**, *134*, 17396−17399.

DOI: 10.1021/acsphotonics.5b00428
ACS Photonics 2016, 3, 158−173

(58) Lee, M. M.; Teuscher, J.; Miyasaka, T.; Murakami, T. N.; Snaith, H. J. Efficient Hybrid Solar Cells Based on Meso-Superstructured Organometal Halide Perovskites. *Science* **2012**, *338*, 643−647.
(59) Carnie, M. J.; Charbonneau, C.; Davies, M. L.; Troughton, J.; Watson, T. M.; Wojciechowski, K.; Snaith, H.; Worsley, D. A. A One-Step Low Temperature Processing Route for Organolead Halide Perovskite Solar Cells. *Chem. Commun.* **2013**, *49*, 7893−7895.
(60) Ball, J. M.; Lee, M. M.; Hey, A.; Snaith, H. J. Low-Temperature Processed Meso-Superstructured to Thin-Film Perovskite Solar Cells. *Energy Environ. Sci.* **2013**, *6*, 1739−1743.
(61) Shi, D.; Adinolfi, V.; Comin, R.; Yuan, M.; Alarousu, E.; Buin, A.; Chen, Y.; Hoogland, S.; Rothenberger, A.; Katsiev, K.; Losovyj, Y.; Zhang, X.; Dowben, P. A.; Mohammed, O. F.; Sargent, E. H.; Bakr, O. M. Low Trap-State Density and Long Carrier Diffusion in Organolead Trihalide Perovskite Single Crystals. *Science* **2015**, *347*, 519−522.
(62) Nie, W.; Tsai, H.; Asadpour, R.; Blancon, J.-C.; Neukirch, A. J.; Gupta, G.; Crochet, J. J.; Chhowalla, M.; Tretiak, S.; Alam, M. A.; Wang, H.-L.; Mohite, A. D. High-Efficiency Solution-Processed Perovskite Solar Cells with Millimeter-Scale Grains. *Science* **2015**, *347*, 522−525.
(63) Yablonovitch, E. Statistical Ray Optics. *J. Opt. Soc. Am.* **1982**, *72*, 899.
(64) Goetzberger, A. Optical Confinement in Thin Si-Solar Cells by Diffuse Back Reflectors. *Proceedings of the 15th IEEE Photovoltaics Specialists Conference* **1981**, 867−870.
(65) Campbell, P.; Green, M. A. The Limiting Efficiency of Silicon Solar Cells under Concentrated Sunlight. *IEEE Trans. Electron Devices* **1986**, *33*, 234−239.
(66) Hägglund, C.; Apell, S. P.; Kasemo, B. Maximized Optical Absorption in Ultrathin Films and Its Application to Plasmon-Based Two-Dimensional Photovoltaics. *Nano Lett.* **2010**, *10*, 3135−3141.
(67) Yu, Z.; Raman, A.; Fan, S. Fundamental Limit of Nanophotonic Light Trapping in Solar Cells. *Proc. Natl. Acad. Sci. U. S. A.* **2010**, *107*, 17491−17496.
(68) Callahan, D. M.; Munday, J. N.; Atwater, H. A. Solar Cell Light Trapping beyond the Ray Optic Limit. *Nano Lett.* **2012**, *12*, 214−218.
(69) Schuster, C. S.; Bozzola, A.; Andreani, L. C.; Krauss, T. F. How to Assess Light Trapping Structures versus a Lambertian Scatterer for Solar Cells? *Opt. Express* **2014**, *22*, A542.
(70) Lal, S.; Link, S.; Halas, N. J. Nano-Optics from Sensing to Waveguiding. *Nat. Photonics* **2007**, *1*, 641−648.
(71) Kabashin, A. V.; Evans, P.; Pastkovsky, S.; Hendren, W.; Wurtz, G. A.; Atkinson, R.; Pollard, R.; Podolskiy, V. A.; Zayats, A. V. Plasmonic Nanorod Metamaterials for Biosensing. *Nat. Mater.* **2009**, *8*, 867−871.
(72) Liu, N.; Weiss, T.; Mesch, M.; Langguth, L.; Eigenthaler, U.; Hirscher, M.; Sönnichsen, C.; Giessen, H. Planar Metamaterial Analogue of Electromagnetically Induced Transparency for Plasmonic Sensing. *Nano Lett.* **2010**, *10*, 1103−1107.
(73) Kwon, M.-K.; Kim, J.-Y.; Kim, B.-H.; Park, I.-K.; Cho, C.-Y.; Byeon, C. C.; Park, S.-J. Surface-Plasmon-Enhanced Light-Emitting Diodes. *Adv. Mater.* **2008**, *20*, 1253−1257.
(74) Okamoto, K.; Niki, I.; Shvartser, A.; Narukawa, Y.; Mukai, T.; Scherer, A. Surface-Plasmon-Enhanced Light Emitters Based on InGaN Quantum Wells. *Nat. Mater.* **2004**, *3*, 601−605.
(75) Vuckovic, J.; Loncar, M.; Scherer, A. Surface Plasmon Enhanced Light-Emitting Diode. *IEEE J. Quantum Electron.* **2000**, *36*, 1131−1144.
(76) Oulton, R. F.; Sorger, V. J.; Zentgraf, T.; Ma, R.-M.; Gladden, C.; Dai, L.; Bartal, G.; Zhang, X. Plasmon Lasers at Deep Subwavelength Scale. *Nature* **2009**, *461*, 629−632.
(77) Ma, R.-M.; Oulton, R. F.; Sorger, V. J.; Bartal, G.; Zhang, X. Room-Temperature Sub-Diffraction-Limited Plasmon Laser by Total Internal Reflection. *Nat. Mater.* **2011**, *10*, 110−113.
(78) Gather, M. C. A Rocky Road to Plasmonic Lasers. *Nat. Photonics* **2012**, *6*, 708−708.
(79) Konstantatos, G.; Sargent, E. H. Nanostructured Materials for Photon Detection. *Nat. Nanotechnol.* **2010**, *5*, 391−400.
(80) Zia, R.; Schuller, J. A.; Chandran, A.; Brongersma, M. L. Plasmonics: The next Chip-Scale Technology. *Mater. Today* **2006**, *9*, 20−27.
(81) Atwater, H. A.; Polman, A. Plasmonics for Improved Photovoltaic Devices. *Nat. Mater.* **2010**, *9*, 205−213.
(82) Pillai, S.; Green, M. A. Plasmonics for Photovoltaic Applications. *Sol. Energy Mater. Sol. Cells* **2010**, *94*, 1481−1486.
(83) Santbergen, R.; Temple, T. L.; Liang, R.; Smets, A. H. M.; van Swaaij, R. A. C. M. M.; Zeman, M. Application of Plasmonic Silver Island Films in Thin-Film Silicon Solar Cells. *J. Opt.* **2012**, *14*, 024010.
(84) Ferry, V. E.; Munday, J. N.; Atwater, H. A. Design Considerations for Plasmonic Photovoltaics. *Adv. Mater.* **2010**, *22*, 4794−4808.
(85) Nakayama, K.; Tanabe, K.; Atwater, H. A. Plasmonic Nanoparticle Enhanced Light Absorption in GaAs Solar Cells. *Appl. Phys. Lett.* **2008**, *93*, 121904.
(86) Green, M. A.; Pillai, S. Harnessing Plasmonics for Solar Cells. *Nat. Photonics* **2012**, *6*, 130−132.
(87) Ferry, V. E.; Sweatlock, L. A.; Pacifici, D.; Atwater, H. A. Plasmonic Nanostructure Design for Efficient Light Coupling into Solar Cells. *Nano Lett.* **2008**, *8*, 4391−4397.
(88) Ferry, V. E.; Verschuuren, M. A.; Li, H. B. T.; Schropp, R. E. I.; Atwater, H. A.; Polman, A. Improved Red-Response in Thin Film a-Si:H Solar Cells with Soft-Imprinted Plasmonic Back Reflectors. *Appl. Phys. Lett.* **2009**, *95*, 183503.
(89) Giannini, V.; Zhang, Y.; Forcales, M.; Gómez Rivas, J. Long-Range Surface Polaritons in Ultra-Thin Films of Silicon. *Opt. Express* **2008**, *16*, 19674.
(90) Chen, X.; Jia, B.; Saha, J. K.; Cai, B.; Stokes, N.; Qiao, Q.; Wang, Y.; Shi, Z.; Gu, M. Broadband Enhancement in Thin-Film Amorphous Silicon Solar Cells Enabled by Nucleated Silver Nanoparticles. *Nano Lett.* **2012**, *12*, 2187−2192.
(91) Wang, Y.; Sun, T.; Paudel, T.; Zhang, Y.; Ren, Z.; Kempa, K. Metamaterial-Plasmonic Absorber Structure for High Efficiency Amorphous Silicon Solar Cells. *Nano Lett.* **2012**, *12*, 440−445.
(92) Tan, H.; Santbergen, R.; Smets, A. H. M.; Zeman, M. Plasmonic Light Trapping in Thin-Film Silicon Solar Cells with Improved Self-Assembled Silver Nanoparticles. *Nano Lett.* **2012**, *12*, 4070−4076.
(93) Wang, D. H.; Kim, D. Y.; Choi, K. W.; Seo, J. H.; Im, S. H.; Park, J. H.; Park, O. O.; Heeger, A. J. Enhancement of Donor-Acceptor Polymer Bulk Heterojunction Solar Cell Power Conversion Efficiencies by Addition of Au Nanoparticles. *Angew. Chem., Int. Ed.* **2011**, *50*, 5519−5523.
(94) Wang, D. H.; Park, K. H.; Seo, J. H.; Seifter, J.; Jeon, J. H.; Kim, J. K.; Park, J. H.; Park, O. O.; Heeger, A. J. Enhanced Power Conversion Efficiency in PCDTBT/PC70BM Bulk Heterojunction Photovoltaic Devices with Embedded Silver Nanoparticle Clusters. *Adv. Energy Mater.* **2011**, *1*, 766−770.
(95) Wang, C. C. D.; Choy, W. C. H.; Duan, C.; Fung, D. D. S.; Sha, W. E. I.; Xie, F.-X.; Huang, F.; Cao, Y. Optical and Electrical Effects of Gold Nanoparticles in the Active Layer of Polymer Solar Cells. *J. Mater. Chem.* **2012**, *22*, 1206−1211.
(96) Chueh, C.-C.; Li, C.-Z.; Jen, A. K.-Y. Recent Progress and Perspective in Solution-Processed Interfacial Materials for Efficient and Stable Polymer and Organometal Perovskite Solar Cells. *Energy Environ. Sci.* **2015**, *8*, 1160−1189.
(97) Gan, Q.; Bartoli, F. J.; Kafafi, Z. H. Plasmonic-Enhanced Organic Photovoltaics: Breaking the 10% Efficiency Barrier. *Adv. Mater.* **2013**, *25*, 2385−2396.
(98) You, J.; Li, X.; Xie, F.; Sha, W. E. I.; Kwong, J. H. W.; Li, G.; Choy, W. C. H.; Yang, Y. Surface Plasmon and Scattering-Enhanced Low-Bandgap Polymer Solar Cell by a Metal Grating Back Electrode. *Adv. Energy Mater.* **2012**, *2*, 1203−1207.
(99) Li, X.; Choy, W. C. H.; Huo, L.; Xie, F.; Sha, W. E. I.; Ding, B.; Guo, X.; Li, Y.; Hou, J.; You, J.; Yang, Y. Dual Plasmonic Nanostructures for High Performance Inverted Organic Solar Cells. *Adv. Mater.* **2012**, *24*, 3046−3052.

DOI: 10.1021/acsphotonics.5b00428
ACS Photonics 2016, 3, 158−173

(100) Mendes, M. J.; Morawiec, S.; Simone, F.; Priolo, F.; Crupi, I. Colloidal Plasmonic Back Reflectors for Light Trapping in Solar Cells. *Nanoscale* **2014**, *6*, 4796−4805.
(101) Haidari, G.; Hajimahmoodzadeh, M.; Fallah, H. R.; Varnamkhasti, M. G. Effective Medium Analysis of Thermally Evaporated Ag Nanoparticle Films for Plasmonic Enhancement in Organic Solar Cell. *Superlattices Microstruct.* **2015**, *85*, 294−304.
(102) Haidari, G.; Hajimahmoodzadeh, M.; Fallah, H. R.; Peukert, A.; Chanaewa, A.; von Hauff, E. Thermally Evaporated Ag Nanoparticle Films for Plasmonic Enhancement in Organic Solar Cells: Effects of Particle Geometry. *Phys. Status Solidi RRL* **2015**, *9*, 161−165.
(103) Niesen, B.; Rand, B. P.; Van Dorpe, P.; Cheyns, D.; Tong, L.; Dmitriev, A.; Heremans, P. Plasmonic Efficiency Enhancement of High Performance Organic Solar Cells with a Nanostructured Rear Electrode. *Adv. Energy Mater.* **2013**, *3*, 145−150.
(104) Jung, K.; Song, H.-J.; Lee, G.; Ko, Y.; Ahn, K.; Choi, H.; Kim, J. Y.; Ha, K.; Song, J.; Lee, J.-K.; Lee, C.; Choi, M. Plasmonic Organic Solar Cells Employing Nanobump Assembly via Aerosol-Derived Nanoparticles. *ACS Nano* **2014**, *8*, 2590−2601.
(105) Beck, F. J.; Stavrinadis, A.; Diedenhofen, S. L.; Lasanta, T.; Konstantatos, G. Surface Plasmon Polariton Couplers for Light Trapping in Thin-Film Absorbers and Their Application to Colloidal Quantum Dot Optoelectronics. *ACS Photonics* **2014**, *1*, 1197−1205.
(106) Salvador, M.; MacLeod, B. A.; Hess, A.; Kulkarni, A. P.; Munechika, K.; Chen, J. I. L.; Ginger, D. S. Electron Accumulation on Metal Nanoparticles in Plasmon-Enhanced Organic Solar Cells. *ACS Nano* **2012**, *6*, 10024−10032.
(107) Paz-Soldan, D.; Lee, A.; Thon, S. M.; Adachi, M. M.; Dong, H.; Maraghechi, P.; Yuan, M.; Labelle, A. J.; Hoogland, S.; Liu, K.; Kumacheva, E.; Sargent, E. H. Jointly Tuned Plasmonic−Excitonic Photovoltaics Using Nanoshells. *Nano Lett.* **2013**, *13*, 1502−1508.
(108) Saliba, M.; Zhang, W.; Burlakov, V. M.; Stranks, S. D.; Sun, Y.; Ball, J. M.; Johnston, M. B.; Goriely, A.; Wiesner, U.; Snaith, H. J. Plasmonic-Induced Photon Recycling in Metal Halide Perovskite Solar Cells. *Adv. Funct. Mater.* **2015**, *25*, 503810.1002/adfm.201500669.
(109) Kulkarni, A. P.; Noone, K. M.; Munechika, K.; Guyer, S. R.; Ginger, D. S. Plasmon-Enhanced Charge Carrier Generation in Organic Photovoltaic Films Using Silver Nanoprisms. *Nano Lett.* **2010**, *10*, 1501−1505.
(110) Echtermeyer, T. J.; Britnell, L.; Jasnos, P. K.; Lombardo, A.; Gorbachev, R. V.; Grigorenko, A. N.; Geim, A. K.; Ferrari, A. C.; Novoselov, K. S. Strong Plasmonic Enhancement of Photovoltage in Graphene. *Nat. Commun.* **2011**, *2*, 458.
(111) Chen, F.-C.; Wu, J.-L.; Lee, C.-L.; Hong, Y.; Kuo, C.-H.; Huang, M. H. Plasmonic-Enhanced Polymer Photovoltaic Devices Incorporating Solution-Processable Metal Nanoparticles. *Appl. Phys. Lett.* **2009**, *95*, 013305.
(112) Yoon, W.-J.; Jung, K.-Y.; Liu, J.; Duraisamy, T.; Revur, R.; Teixeira, F. L.; Sengupta, S.; Berger, P. R. Plasmon-Enhanced Optical Absorption and Photocurrent in Organic Bulk Heterojunction Photovoltaic Devices Using Self-Assembled Layer of Silver Nanoparticles. *Sol. Energy Mater. Sol. Cells* **2010**, *94*, 128−132.
(113) Lindquist, N. C.; Luhman, W. A.; Oh, S.-H.; Holmes, R. J. Plasmonic Nanocavity Arrays for Enhanced Efficiency in Organic Photovoltaic Cells. *Appl. Phys. Lett.* **2008**, *93*, 123308.
(114) Akimov, Y. A.; Ostrikov, K.; Li, E. P. Surface Plasmon Enhancement of Optical Absorption in Thin-Film Silicon Solar Cells. *Plasmonics* **2009**, *4*, 107−113.
(115) Hägglund, C.; Zeltzer, G.; Ruiz, R.; Thomann, I.; Lee, H.-B.-R.; Brongersma, M. L.; Bent, S. F. Self-Assembly Based Plasmonic Arrays Tuned by Atomic Layer Deposition for Extreme Visible Light Absorption. *Nano Lett.* **2013**, *13*, 3352−3357.
(116) Han, S. E.; Chen, G. Toward the Lambertian Limit of Light Trapping in Thin Nanostructured Silicon Solar Cells. *Nano Lett.* **2010**, *10*, 4692−4696.
(117) Yu, Z.; Raman, A.; Fan, S. Fundamental Limit of Nanophotonic Light Trapping in Solar Cells. *Proc. Natl. Acad. Sci. U. S. A.* **2010**, *107*, 17491−17496.
(118) Ciracì, C.; Hill, R. T.; Mock, J. J.; Urzhumov, Y.; Fernández-Domínguez, A. I.; Maier, S. A.; Pendry, J. B.; Chilkoti, A.; Smith, D. R. Probing the Ultimate Limits of Plasmonic Enhancement. *Science* **2012**, *337*, 1072−1074.
(119) Karatay, D. U.; Salvador, M.; Yao, K.; Jen, A. K.-Y.; Ginger, D. S. Performance Limits of Plasmon-Enhanced Organic Photovoltaics. *Appl. Phys. Lett.* **2014**, *105*, 033304.
(120) Marklund, M.; Brodin, G.; Stenflo, L.; Liu, C. S. New Quantum Limits in Plasmonic Devices. *EPL Europhys. Lett.* **2008**, *84*, 17006.
(121) Wu, J.-L.; Chen, F.-C.; Hsiao, Y.-S.; Chien, F.-C.; Chen, P.; Kuo, C.-H.; Huang, M. H.; Hsu, C.-S. Surface Plasmonic Effects of Metallic Nanoparticles on the Performance of Polymer Bulk Heterojunction Solar Cells. *ACS Nano* **2011**, *5*, 959−967.
(122) Xue, M.; Li, L.; Tremolet de Villers, B. J.; Shen, H.; Zhu, J.; Yu, Z.; Stieg, A. Z.; Pei, Q.; Schwartz, B. J.; Wang, K. L. Charge-Carrier Dynamics in Hybrid Plasmonic Organic Solar Cells with Ag Nanoparticles. *Appl. Phys. Lett.* **2011**, *98*, 253302.
(123) Heo, S. W.; Lee, E. J.; Song, K. W.; Lee, J. Y.; Moon, D. K. Enhanced Carrier Mobility and Photon-Harvesting Property by Introducing Au Nano-Particles in Bulk Heterojunction Photovoltaic Cells. *Org. Electron.* **2013**, *14*, 1931−1938.
(124) Li, X.; Choy, W. C. H.; Lu, H.; Sha, W. E. I.; Ho, A. H. P. Efficiency Enhancement of Organic Solar Cells by Using Shape-Dependent Broadband Plasmonic Absorption in Metallic Nanoparticles. *Adv. Funct. Mater.* **2013**, *23*, 2728−2735.
(125) Kim, W.; Cha, B. G.; Kim, J. K.; Kang, W.; Kim, E.; Ahn, T. K.; Wang, D. H.; Du, Q. G.; Cho, J. H.; Kim, J.; Park, J. H. Tailoring Dispersion and Aggregation of Au Nanoparticles in the BHJ Layer of Polymer Solar Cells: Plasmon Effects versus Electrical Effects. *ChemSusChem* **2014**, *7*, 3452−3458.
(126) Lu, Z.; Pan, X.; Ma, Y.; Li, Y.; Zheng, L.; Zhang, D.; Xu, Q.; Chen, Z.; Wang, S.; Qu, B.; Liu, F.; Huang, Y.; Xiao, L.; Gong, Q. Plasmonic-Enhanced Perovskite Solar Cells Using Alloy Popcorn Nanoparticles. *RSC Adv.* **2015**, *5*, 11175−11179.
(127) Zhang, X.; Zhang, J.; Liu, J.; Johansson, E. M. J. Solution Processed Flexible and Bending Durable Heterojunction Colloidal Quantum Dot Solar Cell. *Nanoscale* **2015**, *7*, 11520−11524.
(128) Yao, X.; Chang, Y.; Li, G.; Mi, L.; Liu, S.; Wang, H.; Yu, Y.; Jiang, Y. Inverted Quantum-Dot Solar Cells with Depleted Heterojunction Structure Employing CdS as the Electron Acceptor. *Sol. Energy Mater. Sol. Cells* **2015**, *137*, 287−292.
(129) Kim, G.-H.; Walker, B.; Kim, H.-B.; Kim, J. Y.; Sargent, E. H.; Park, J.; Kim, J. Y. Inverted Colloidal Quantum Dot Solar Cells. *Adv. Mater.* **2014**, *26*, 3321−3327.
(130) Ning, Z.; Voznyy, O.; Pan, J.; Hoogland, S.; Adinolfi, V.; Xu, J.; Li, M.; Kirmani, A. R.; Sun, J.-P.; Minor, J.; Kemp, K. W.; Dong, H.; Rollny, L.; Labelle, A.; Carey, G.; Sutherland, B.; Hill, I.; Amassian, A.; Liu, H.; Tang, J.; Bakr, O. M.; Sargent, E. H. Air-Stable N-Type Colloidal Quantum Dot Solids. *Nat. Mater.* **2014**, *13*, 822−828.
(131) Shen, C.; Tong, H.; Gao, W.; Yuan, S.; Chen, G.; Yang, Y. Effects of Anode Structures and Fabrication Methods on Cell Efficiencies of CdS/CdSe Quantum Dot Co-Sensitized Solar Cells. *J. Alloys Compd.* **2015**, *644*, 205−210.
(132) Lan, X.; Masala, S.; Sargent, E. H. Charge-Extraction Strategies for Colloidal Quantum Dot Photovoltaics. *Nat. Mater.* **2014**, *13*, 233−240.
(133) Maraghechi, P.; Labelle, A. J.; Kirmani, A. R.; Lan, X.; Adachi, M. M.; Thon, S. M.; Hoogland, S.; Lee, A.; Ning, Z.; Fischer, A.; Amassian, A.; Sargent, E. H. The Donor−Supply Electrode Enhances Performance in Colloidal Quantum Dot Solar Cells. *ACS Nano* **2013**, *7*, 6111−6116.
(134) Kholmicheva, N.; Moroz, P.; Rijal, U.; Bastola, E.; Uprety, P.; Liyanage, G.; Razgoniaev, A.; Ostrowski, A. D.; Zamkov, M. Plasmonic Nanocrystal Solar Cells Utilizing Strongly Confined Radiation. *ACS Nano* **2014**, *8*, 12549−12559.
(135) Beck, F. J.; Lasanta, T.; Konstantatos, G. Plasmonic Schottky Nanojunctions for Tailoring the Photogeneration Profile in Thin Film Solar Cells. *Adv. Opt. Mater.* **2014**, *2*, 493−500.

DOI: 10.1021/acsphotonics.5b00428
ACS Photonics 2016, 3, 158−173

(136) Gee, J. M. The Effect of Parasitic Absorption Losses on Light Trapping in Thin Silicon Solar Cells. In *Conference Record of the Twentieth IEEE Photovoltaic Specialists Conference*, 1988; 1988; Vol. *1*, pp 549−554.
(137) Paetzold, U. W.; Hallermann, F.; Pieters, B. E.; Rau, U.; Carius, R.; von Plessen, G. *Proc. SPIE*; **2010**; Vol. *7725*, pp 772517−772517−910.1117/12.854430.
(138) Khurgin, J. B.; Boltasseva, A. Reflecting upon the Losses in Plasmonics and Metamaterials. *MRS Bull.* **2012**, *37*, 768−779.
(139) Palanchoke, U.; Jovanov, V.; Kurz, H.; Dewan, R.; Magnus, P.; Stiebig, H.; Knipp, D. Influence of Back Contact Roughness on Light Trapping and Plasmonic Losses of Randomly Textured Amorphous Silicon Thin Film Solar Cells. *Appl. Phys. Lett.* **2013**, *102*, 083501.
(140) Du, P.; Jing, P.; Li, D.; Cao, Y.; Liu, Z.; Sun, Z. Plasmonic Ag@ Oxide Nanoprisms for Enhanced Performance of Organic Solar Cells. *Small* **2015**, *11*, 2454−2462.
(141) Wu, B.; Mathews, N.; Sum, T. C. *Proc. SPIE* SPIE OPTO 2014; Vol. *8981*, pp 898111−898111−10.10.1117/12.2037744
(142) Mandoc, M. M.; Veurman, W.; Koster, L. J. A.; de Boer, B.; Blom, P. W. M. Origin of the Reduced Fill Factor and Photocurrent in MDMO-PPV:PCNEPV All-Polymer Solar Cells. *Adv. Funct. Mater.* **2007**, *17*, 2167−2173.
(143) Scholl, J. A.; Koh, A. L.; Dionne, J. A. Quantum Plasmon Resonances of Individual Metallic Nanoparticles. *Nature* **2012**, *483*, 421−427.
(144) Oldenburg, S. J.; Averitt, R. D.; Westcott, S. L.; Halas, N. J. Nanoengineering of Optical Resonances. *Chem. Phys. Lett.* **1998**, *288*, 243−247.
(145) Mock, J. J.; Barbic, M.; Smith, D. R.; Schultz, D. A.; Schultz, S. Shape Effects in Plasmon Resonance of Individual Colloidal Silver Nanoparticles. *J. Chem. Phys.* **2002**, *116*, 6755−6759.
(146) Mock, J. J.; Smith, D. R.; Schultz, S. Local Refractive Index Dependence of Plasmon Resonance Spectra from Individual Nanoparticles. *Nano Lett.* **2003**, *3*, 485−491.
(147) Hutter, E.; Fendler, J. H. Exploitation of Localized Surface Plasmon Resonance. *Adv. Mater.* **2004**, *16*, 1685−1706.
(148) Bruggeman, D. A. G. Dielectric Constant and Conductivity of Mixtures of Isotropic Materials. *Ann. Phys.* **1935**, *24*, 636−679.
(149) Garnett, J. C. M. Colours in Metal Glasses, in Metallic Films, and in Metallic Solutions. II. *Philos. Trans. R. Soc., A* **1906**, *205*, 237−288.
(150) Hulst, H. C.; Van De Hulst, H. C. *Light Scattering by Small Particles*; Courier Corporation, 1957.
(151) Fu, Q.; Sun, W. Mie Theory for Light Scattering by a Spherical Particle in an Absorbing Medium. *Appl. Opt.* **2001**, *40*, 1354.
(152) Futamata, M.; Maruyama, Y.; Ishikawa, M. Local Electric Field and Scattering Cross Section of Ag Nanoparticles under Surface Plasmon Resonance by Finite Difference Time Domain Method. *J. Phys. Chem. B* **2003**, *107*, 7607−7617.
(153) Ni, W.; Kou, X.; Yang, Z.; Wang, J. Tailoring Longitudinal Surface Plasmon Wavelengths, Scattering and Absorption Cross Sections of Gold Nanorods. *ACS Nano* **2008**, *2*, 677−686.
(154) Draine, B. T.; Flatau, P. J. Discrete-Dipole Approximation for Scattering Calculations. *J. Opt. Soc. Am. A* **1994**, *11*, 1491.
(155) Jin, J.-M.; Liepa, V. V. Application of Hybrid Finite Element Method to Electromagnetic Scattering from Coated Cylinders. *IEEE Trans. Antennas Propag.* **1988**, *36*, 50−54.
(156) Swinehart, D. F. The Beer-Lambert Law. *J. Chem. Educ.* **1962**, *39*, 333.
(157) Taflove, A.; Hagness, S. C. *Computational Electrodynamics: The Finite-Difference Time-Domain Method*, 3rd ed..; Artech House: Boston, MA, 2005.
(158) Emmott, C. J. M.; Röhr, J. A.; Campoy-Quiles, M.; Kirchartz, T.; Urbina, A.; Ekins-Daukes, N. J.; Nelson, J. Organic Photovoltaic Greenhouses: A Unique Application for Semi-Transparent PV? *Energy Environ. Sci.* **2015**, *8*, 1317−1328.
(159) Löper, P.; Stuckelberger, M.; Niesen, B.; Werner, J.; Filipič, M.; Moon, S.-J.; Yum, J.-H.; Topič, M.; De Wolf, S.; Ballif, C. Complex Refractive Index Spectra of CH3NH3PbI3 Perovskite Thin Films Determined by Spectroscopic Ellipsometry and Spectrophotometry. *J. Phys. Chem. Lett.* **2015**, *6*, 66−71.
(160) Gollu, S. R.; Murthy, M. S.; Sharma, R.; Srinivas, G.; Ganguly, S.; Gupta, D. Enhanced Efficiency of Inverted Bulk Heterojunction Solar Cells with Embedded Silica Nanoparticles. In *Photovoltaic Specialist Conference (PVSC), 2014 IEEE 40th*; 2014; pp 1745−1749.
(161) Fofang, N. T.; Luk, T. S.; Okandan, M.; Nielson, G. N.; Brener, I. Substrate-Modified Scattering Properties of Silicon Nanostructures for Solar Energy Applications. *Opt. Express* **2013**, *21*, 4774.
(162) Tanev, S.; Tuchin, V. V.; Paddon, P. Light Scattering Effects of Gold Nanoparticles in Cells: FDTD Modeling. *Laser Phys. Lett.* **2006**, *3*, 594.
(163) Jiang, S.; Hu, Z.; Chen, Z.; Fu, X.; Jiang, X.; Jiao, Q.; Yu, T.; Zhang, G. Resonant Absorption and Scattering Suppression of Localized Surface Plasmons in Ag Particles on Green LED. *Opt. Express* **2013**, *21*, 12100.
(164) Chen, H.; Kou, X.; Yang, Z.; Ni, W.; Wang, J. Shape- and Size-Dependent Refractive Index Sensitivity of Gold Nanoparticles. *Langmuir* **2008**, *24*, 5233−5237.
(165) Lee, K.-S.; El-Sayed, M. A. Dependence of the Enhanced Optical Scattering Efficiency Relative to That of Absorption for Gold Metal Nanorods on Aspect Ratio, Size, End-Cap Shape, and Medium Refractive Index. *J. Phys. Chem. B* **2005**, *109*, 20331−20338.
(166) Li, M.; Cushing, S. K.; Zhang, J.; Lankford, J.; Aguilar, Z. P.; Ma, D.; Wu, N. Shape-Dependent Surface-Enhanced Raman Scattering in gold−Raman-Probe−silica Sandwiched Nanoparticles for Biocompatible Applications. *Nanotechnology* **2012**, *23*, 115501.
(167) Wang, X.; Liu, X.; Yin, D.; Ke, Y.; Swihart, M. T. Size-, Shape-, and Composition-Controlled Synthesis and Localized Surface Plasmon Resonance of Copper Tin Selenide Nanocrystals. *Chem. Mater.* **2015**, *27*, 3378−3388.
(168) Zhu, J.; Huang, L.; Zhao, J.; Wang, Y.; Zhao, Y.; Hao, L.; Lu, Y. Shape Dependent Resonance Light Scattering Properties of Gold Nanorods. *Mater. Sci. Eng., B* **2005**, *121*, 199−203.
(169) Zhu, J. Shape Dependent Full Width at Half Maximum of the Absorption Band in Gold Nanorods. *Phys. Lett. A* **2005**, *339*, 466−471.
(170) Jain, P. K.; Lee, K. S.; El-Sayed, I. H.; El-Sayed, M. A. Calculated Absorption and Scattering Properties of Gold Nanoparticles of Different Size, Shape, and Composition: Applications in Biological Imaging and Biomedicine. *J. Phys. Chem. B* **2006**, *110*, 7238−7248.
(171) Tao, A.; Sinsermsuksakul, P.; Yang, P. Polyhedral Silver Nanocrystals with Distinct Scattering Signatures. *Angew. Chem., Int. Ed.* **2006**, *45*, 4597−4601.
(172) Evanoff, D. D.; Chumanov, G. Synthesis and Optical Properties of Silver Nanoparticles and Arrays. *ChemPhysChem* **2005**, *6*, 1221−1231.
(173) Carretero-Palacios, S.; Calvo, M. E.; Miguez, H. Absorption Enhancement in Organic-Inorganic Halide Perovskite Films with Embedded Plasmonic Gold Nanoparticles. *J. Phys. Chem. C* **2015**, *119*, 18635.
(174) García de Arquer, F. P.; Beck, F. J.; Konstantatos, G. Absorption Enhancement in Solution Processed Metal-Semiconductor Nanocomposites. *Opt. Express* **2011**, *19*, 21038.
(175) Pettersson, L. A. A.; Roman, L. S.; Inganäs, O. Modeling Photocurrent Action Spectra of Photovoltaic Devices Based on Organic Thin Films. *J. Appl. Phys.* **1999**, *86*, 487−496.
(176) Burkhard, G. F.; Hoke, E. T.; McGehee, M. D. Accounting for Interference, Scattering, and Electrode Absorption to Make Accurate Internal Quantum Efficiency Measurements in Organic and Other Thin Solar Cells. *Adv. Mater.* **2010**, *22*, 3293−3297.
(177) Kern, R.; Sastrawan, R.; Ferber, J.; Stangl, R.; Luther, J. Modeling and Interpretation of Electrical Impedance Spectra of Dye Solar Cells Operated under Open-Circuit Conditions. *Electrochim. Acta* **2002**, *47*, 4213−4225.
(178) Basore, P. A. Numerical Modeling of Textured Silicon Solar Cells Using PC-1D. *IEEE Trans. Electron Devices* **1990**, *37*, 337−343.
(179) Ferber, J.; Stangl, R.; Luther, J. An Electrical Model of the Dye-Sensitized Solar Cell. *Sol. Energy Mater. Sol. Cells* **1998**, *53*, 29−54.

DOI: 10.1021/acsphotonics.5b00428
ACS Photonics 2016, 3, 158−173

(180) MacKenzie, R. C. I.; Kirchartz, T.; Dibb, G. F. A.; Nelson, J. Modeling Nongeminate Recombination in P3HT:PCBM Solar Cells. *J. Phys. Chem. C* **2011**, *115*, 9806−9813.
(181) Li, W.; Hendriks, K. H.; Roelofs, W. S. C.; Kim, Y.; Wienk, M. M.; Janssen, R. A. J. Efficient Small Bandgap Polymer Solar Cells with High Fill Factors for 300 Nm Thick Films. *Adv. Mater.* **2013**, *25*, 3182−3186.

DOI: 10.1021/acsphotonics.5b00428
ACS Photonics 2016, 3, 158−173